Article

Neuron

A Disinhibitory Microcircuit Mediates Conditioned Social Fear in the Prefrontal Cortex

Graphical Abstract

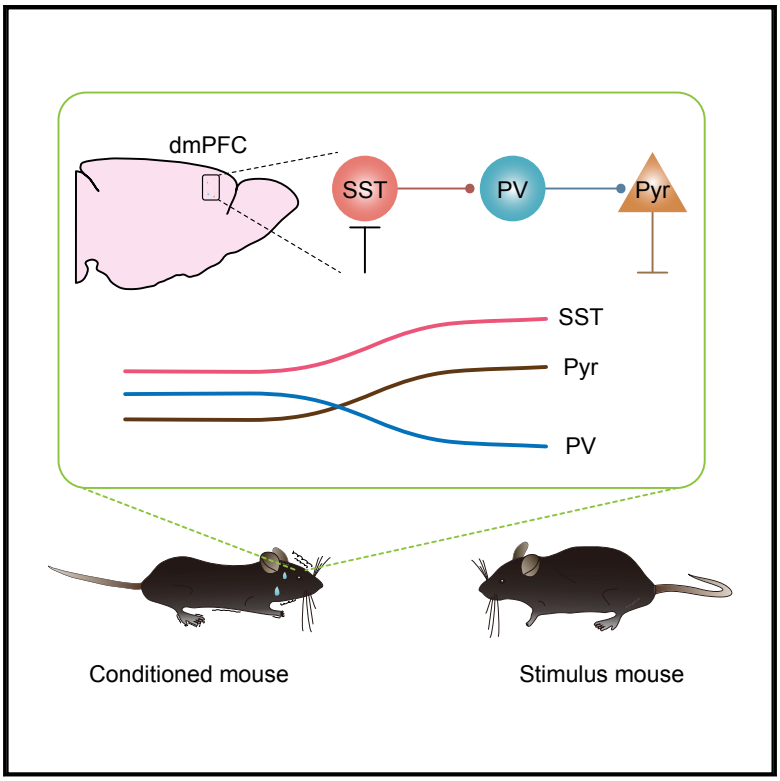

Authors

Haifeng Xu, Ling Liu, Yuanyuan Tian, ..., Tian-Le Xu, Shumin Duan, Han Xu

Correspondence

xuhan2014@zju.edu.cn

In Brief

Prefrontal cortex plays an essential role in fear expression. Xu et al. reveal a disinhibitory microcircuit in prefrontal cortex through interactions between interneuron subtypes and suggest that SST INs-mediated disinhibition represents an important circuit mechanism in gating social fear behavior.

Highlights

- Social fear conditioning induces robust and specific social fear in mice
- The dmPFC participates in social fear expression
- SST INs disinhibit principal neurons via their inhibition of FS-PV INs
- The disinhibitory microcircuitry is crucial for social fear expression

Xu et al., 2019, Neuron *102*, 668–682
May 8, 2019
https://doi.org/10.1016/j.neuron.2019.02.026

CellPress

CellPress

Neuron
Article

A Disinhibitory Microcircuit Mediates Conditioned Social Fear in the Prefrontal Cortex

Haifeng Xu,[1,4] Ling Liu,[1,4] Yuanyuan Tian,[1,4] Jun Wang,[1,4] Jie Li,[1] Junqiang Zheng,[1] Hongfei Zhao,[1] Miao He,[2] Tian-Le Xu,[3] Shumin Duan,[1] and Han Xu[1,5,*]

[1]Center for Neuroscience and Department of Neurology of the Second Affiliated Hospital, NHC and CAMS Key Laboratory of Medical Neurobiology, Zhejiang University School of Medicine, Hangzhou 310058, China
[2]Institute of Brain Science, State Key Laboratory of Medical Neurobiology, and Collaborative Innovation Center for Brain Science, Fudan University, Shanghai 200032, China
[3]Center for Brain Science and Department of Anatomy and Physiology, Shanghai Jiao Tong University School of Medicine, Shanghai 200025, China
[4]These authors contributed equally
[5]Lead Contact
*Correspondence: xuhan2014@zju.edu.cn
https://doi.org/10.1016/j.neuron.2019.02.026

SUMMARY

Fear behavior is under tight control of the prefrontal cortex, but the underlying microcircuit mechanism remains elusive. In particular, it is unclear how distinct subtypes of inhibitory interneurons (INs) within prefrontal cortex interact and contribute to fear expression. We employed a social fear conditioning paradigm and induced robust social fear in mice. We found that social fear is characterized by activation of dorsal medial prefrontal cortex (dmPFC) and is largely diminished by dmPFC inactivation. With a combination of *in vivo* electrophysiological recordings and fiber photometry together with cell-type-specific pharmacogenetics, we further demonstrated that somatostatin (SST) INs suppressed parvalbumin (PV) INs and disinhibited pyramidal cells and consequently enhanced dmPFC output to mediate social fear responses. These results reveal a previously unknown disinhibitory microcircuit in prefrontal cortex through interactions between IN subtypes and suggest that SST INs-mediated disinhibition represents an important circuit mechanism in gating social fear behavior.

INTRODUCTION

Fear is typically an adaptive feeling to an imminent threat and is helpful for animals and humans to avoid danger. Inappropriate fear, on the other hand, is a maladaptive response to environmental stimuli and is commonly observed in a number of psychiatric disorders including posttraumatic stress disorder (PTSD) and anxiety disorders (Buff et al., 2016; Nees et al., 2018; Sheynin et al., 2017). Social fear is one such inappropriate fear and represents a core behavioral symptom of social anxiety disorder (SAD), which is prevalent worldwide and causes disabling effects (American Psychiatric Association, 2013). The pathological mechanism for SAD is poorly understood and there are no satisfactory therapeutic options available (Stein and Stein, 2008). It has been well established that the amygdala plays a determinant role in the control of fear and anxiety (Phelps and LeDoux, 2005). At the same time, the amygdala is under functional regulation of various cortical and subcortical inputs. Recent evidence from both human and animal studies have implicated the prefrontal cortex (PFC) in the processes of fear regulation (Burgos-Robles et al., 2009; Etkin et al., 2011; Karalis et al., 2016). In particular, PFC hyperactivity is tightly linked to excessive and long-lasting fear states in patients with SAD (Buff et al., 2016; Kawashima et al., 2016). To date, however, the neuronal substrates and local microcircuits underlying PFC network excitability and hence social fear expression are still elusive.

Normal brain functions rely on a delicate balance between excitation and inhibition. To perform its complex operations, the mammalian cerebral cortex has evolved a large diversity of GABAergic interneurons (INs) based on differences in neuronal morphologies, electrophysiological properties, and neurochemical markers (Ascoli et al., 2008; Fishell and Rudy, 2011; Rudy et al., 2011; Somogyi and Klausberger, 2005). Different subtypes of inhibitory INs could effectively control cortical network activity via feedforward, feedback inhibition, and/or disinhibitory mechanisms (Isaacson and Scanziani, 2011; Tremblay et al., 2016; Xu et al., 2013). Moreover, recent evidence demonstrates functional correlates between specific cortical IN subtypes and distinct behaviors in sensory perception, motor integration, space coding, as well as working memory, attention, and reward processing (Kamigaki and Dan, 2017; Kim et al., 2016a, 2016b; Kvitsiani et al., 2013; Lee et al., 2012, 2013; Miao et al., 2017). In contrast, we know much less about the differential participation of cortical inhibitory IN subtypes in the control of emotional behaviors. In particular, it is unclear how distinct subtypes of inhibitory INs within PFC interact and hence contribute to social fear responses. Answers to these questions will not only reveal how PFC contributes to fear behaviors, but will also shed light on what circuit disturbances could cause social dysfunctions.

RESULTS

Conditioned Social Fear in Mice

To induce social fear in mice, we employed a social fear conditioning (SFC) paradigm (Menon et al., 2018; Toth et al., 2012). In brief, a freely moving experimental mouse and a confined stimulus mouse were placed in a conditioning box. After a 2 min exploration, the experimental mouse was then given an electric foot shock each time as it investigated the stimulus mouse during a period of 20 min (Figure 1A; Video S1). Conditioned mice developed robust escape and avoidance behavior when oriented toward a conspecific, indicating successful acquisition of social fear following SFC (Video S2). To quantify social fear behavior, we used a three-chamber social interaction test, which is a widely used assay to examine social behavior in rodents (Figure 1B) (Moy et al., 2004). As compared to unconditioned control mice, those experienced SFC exhibited a dramatic decrease in the time spent in the social chamber (control: 315.3 ± 12.4 s, n = 9; conditioned: 100.1 ± 25.8 s, n = 9; $p < 0.0001$), the social interaction index (the difference in the time spent in the social and neutral chambers divided by the total time spent in both chambers) (control: 0.34 ± 0.04, n = 9; conditioned: −0.48 ± 0.12, n = 9; $p < 0.0001$), and times of social approaches (control: 20.1 ± 1.6, n = 9; conditioned: 8.7 ± 1.9, n = 9; $p < 0.001$) (Figures 1C–1E). The social fear behavior was further confirmed with a social preference-avoidance test (Figure 1H). Again, the conditioned mice spent significantly less time with stimulus mouse relative to unconditioned controls (control: 328.5 ± 27.6 s, n = 8; conditioned: 36.1 ± 14.0 s, n = 8; $p < 0.0001$) with a smaller social interaction index (the time spent in the social zone divided by the time spent in corners) (control: 9.75 ± 2.16, n = 8; conditioned: 0.22 ± 0.10, n = 8; $p < 0.001$) and less approach times (control: 34.5 ± 2.3, n = 8; conditioned: 11.4 ± 3.4, n = 8; $p < 0.0001$) (Figures 1I–1K). In addition to the striking reduction in social investigation, conditioned mice approached the stimulus mouse at a slow speed in stretched postures, behavioral indicators of an elevated fear state in rodents, which was not observed in unconditioned control mice (Figures 1F, 1G, 1L, and 1M) (Toth et al., 2012). It is worth noting that the male stimulus mice used in either test were different from the ones used during SFC. And indeed, when stimulus mouse was replaced with a female mouse, the social fear behavior was equally present as well (Figures S1A and S1B). Moreover, conditioned mice also avoided a non-aggressive female mouse that was introduced into their home cage (Figures S1C–S1F). These results indicate that conditioned mice developed fear not only to the particular stimulus mouse associated with conditioning but also to their conspecifics in general even in a natural social setting. In contrast, the conditioned mice did not exhibit fear responses to a novel object (Figures S1G and S1H), suggesting the specificity of fear to social stimulus. Besides, the conditioned mice were not accompanied by changes in locomotion, general anxiety, or depressive-like behaviors (Figure S2). Together, the SFC that we used could induce robust and specific social fear in mice without confounding behavioral alterations and thus represents a suitable animal paradigm to study the neural foundations underlying social fear.

The dmPFC Participates in Social Fear Expression

Human imaging studies demonstrate that patients with SAD show abnormal hyperactivity in PFC (Buff et al., 2016; Kawashima et al., 2016), we therefore next examined PFC neuronal reactions following social fear in conditioned mice. After exposure to a conspecific, a significant increase in the number of c-Fos positive cells was observed in dorsal medial PFC (dmPFC), including the prelimbic subregion (PrL) in mice with conditioned social fear (Figures 2A and 2B).

To determine whether dmPFC activity indeed contributed to social fear expression in conditioned mice, we employed a pharmacological approach with GABAa receptor agonist muscimol (MUS, 0.25 nmol, 150 nL/side) to rapidly inactivate dmPFC neurons in behaving mice (Figure 2C). Three-chamber social interaction test was used to evaluate the effect of dmPFC inactivation on social fear (Figure 2D). When compared with vehicle-treated controls (PBS), mice with MUS injection displayed a significant increase in time spent in the social chamber (PBS: 100.7 ± 25.9 s, n = 8; MUS: 247.1 ± 23.5 s, n = 8; $p < 0.001$), the social interaction index (PBS: −0.53 ± 0.10 s, n = 8; MUS: 0.06 ± 0.10 s, n = 8; $p < 0.01$), and times of social approaches (PBS: 7.8 ± 1.7, n = 8; MUS: 14.6 ± 1.5, n = 8; $p < 0.01$) (Figures 2E–2G). In addition, MUS-injected mice also exhibited significantly less stretched postures (PBS: 10.1 ± 1.5, n = 8; MUS: 1.5 ± 1.0, n = 8; $p < 0.001$) and increased approach speed (PBS: 5.6 ± 0.6 cm/s, n = 8; MUS: 10.5 ± 0.5 cm/s, n = 8; $p < 0.0001$), indicating a direct reduction of fear (Figures 2H and 2I). In comparison, dmPFC inactivation did not change the time spent in the social chamber in unconditioned control mice, suggesting that this manipulation neither nonspecifically increased social preference nor interfered with animals' ability to differentiate between regions of their environment (the social versus neutral chambers) (Figures S3A–S3B). This finding is consistent with previous pharmacological inactivation study conducted in rats (Lungwitz et al., 2014). Together, these results indicated that dmPFC plays an essential role in the expression of social fear behavior. In comparison, consistent with the patterns of c-Fos expression, MUS injection into the IL subregion failed to inhibit social fear, suggesting that IL is not involved in social fear expression (Figures 2J–2P).

We also examined the role of dmPFC in social fear that was elicited by another commonly used paradigm, that is, social defeat (Franklin et al., 2017). After 3 consecutive days of social defeat by CD1 mice, the experimental C57 mice developed social fear behaviors (Figures S4A–S4D). To test whether the social fear induced by social defeat is dependent on dmPFC, we inactivated dmPFC neurons with MUS (0.25 nmol, 150 nL/side). When compared with vehicle-treated controls (PBS), mice with MUS injection spent significantly more time with stimulus mouse in a social preference-avoidance test (Figures S4E–S4H). This result indicated that social fear induced in a more naturalistic way by social defeat is also dependent on dmPFC.

In addition to dmPFC, c-Fos expression was markedly increased in the basolateral amygdala (BLA), and pharmacological inactivation of BLA largely reduced social fear responses (Figure S5). This finding is consistent with the well-established notion that BLA is required for the expression of conditioned fear (Phelps and LeDoux, 2005). Indeed, the BLA inactivation

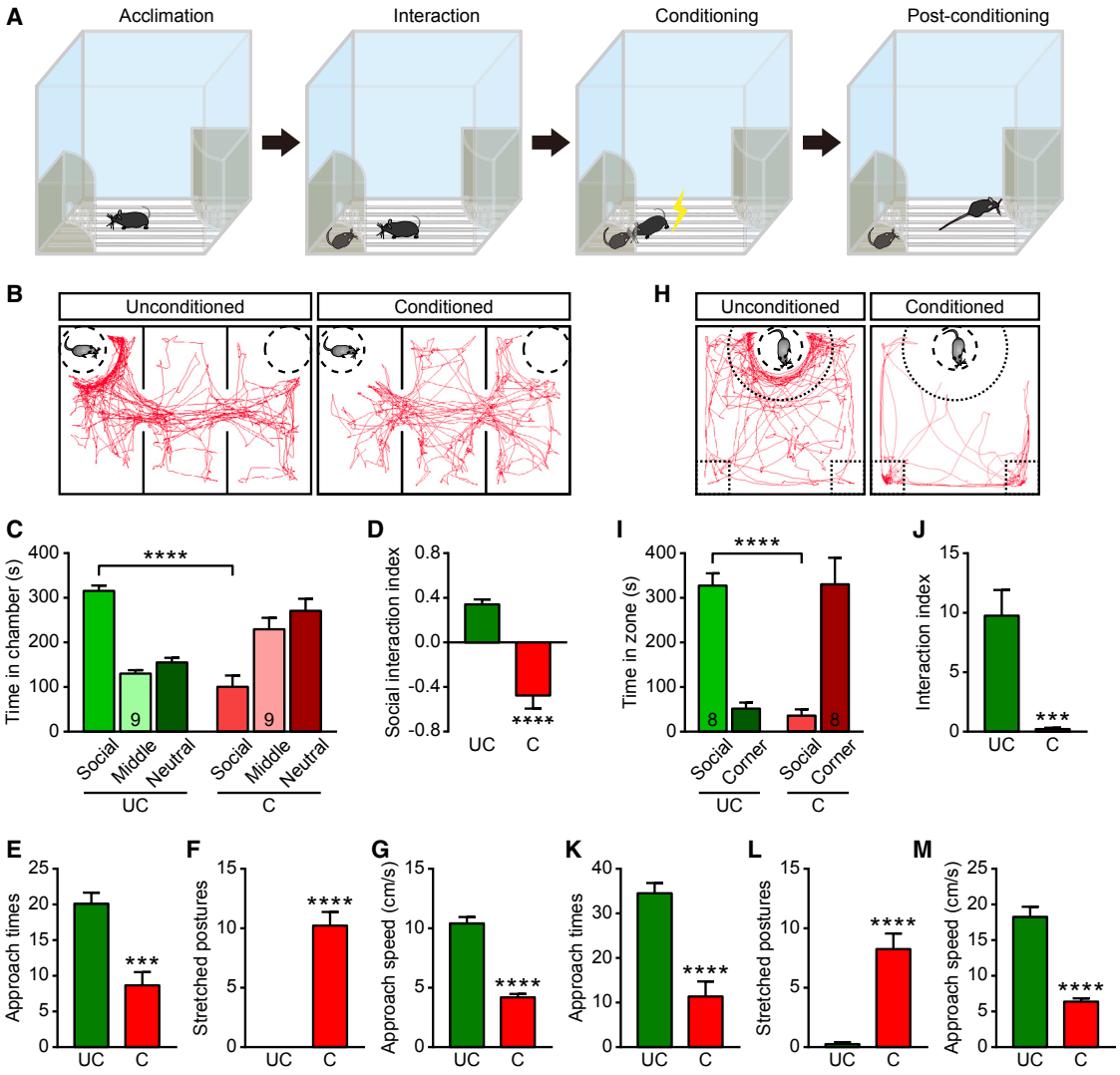

Figure 1. Induction of Social Fear Responses by SFC

(A) Schematic diagram showing the SFC paradigm. The experimental mouse was allowed to freely interact with the stimulus mouse (Interaction) after acclimation to the conditioning chamber (Acclimation) and then was given a foot shock each time it approached and investigated the stimulus mouse (Conditioning).

(B) Representative movement traces showing the locations of an unconditioned control mouse (left) and a social fear conditioned mouse (right) in a three-chamber social interaction test.

(C) Quantification of time spent by unconditioned (UC) and conditioned (C) mice in each chamber. Error bars indicate mean ± SEM. ****$p < 0.0001$; two-way ANOVA, Bonferroni multiple comparison post hoc tests. Numbers in columns indicate the number of mice analyzed.

(D) Social interaction index (the difference in the time spent in the social and neutral chambers divided by the total time spent in both chambers) was significantly smaller in conditioned mice. Error bars indicate mean ± SEM. ****$p < 0.0001$; unpaired t test.

(E–G) Quantification of approach times (E), stretched postures (F), and approach speed (G) of unconditioned and conditioned mice upon approaching stimulus mouse. Error bars indicate mean ± SEM. ***$p < 0.001$; ****$p < 0.0001$; unpaired t test.

(H) Representative movement traces showing the locations of an unconditioned control mouse (left) and a social fear conditioned mouse (right) in a social preference-avoidance test.

(I) Quantification of time spent by unconditioned and conditioned mice in social zone and corners. Error bars indicate mean ± SEM. ****$p < 0.0001$; two-way ANOVA, Bonferroni multiple comparison post hoc tests. Numbers in columns indicate the number of mice analyzed.

(J) Social interaction index (the time spent in the social zone divided by the time spent in corners) was significantly smaller in conditioned mice. ***$p < 0.001$; unpaired t test.

(K–M) The same as (E)–(G) but in an open-field social preference-avoidance test.

See also Figures S1 and S2.

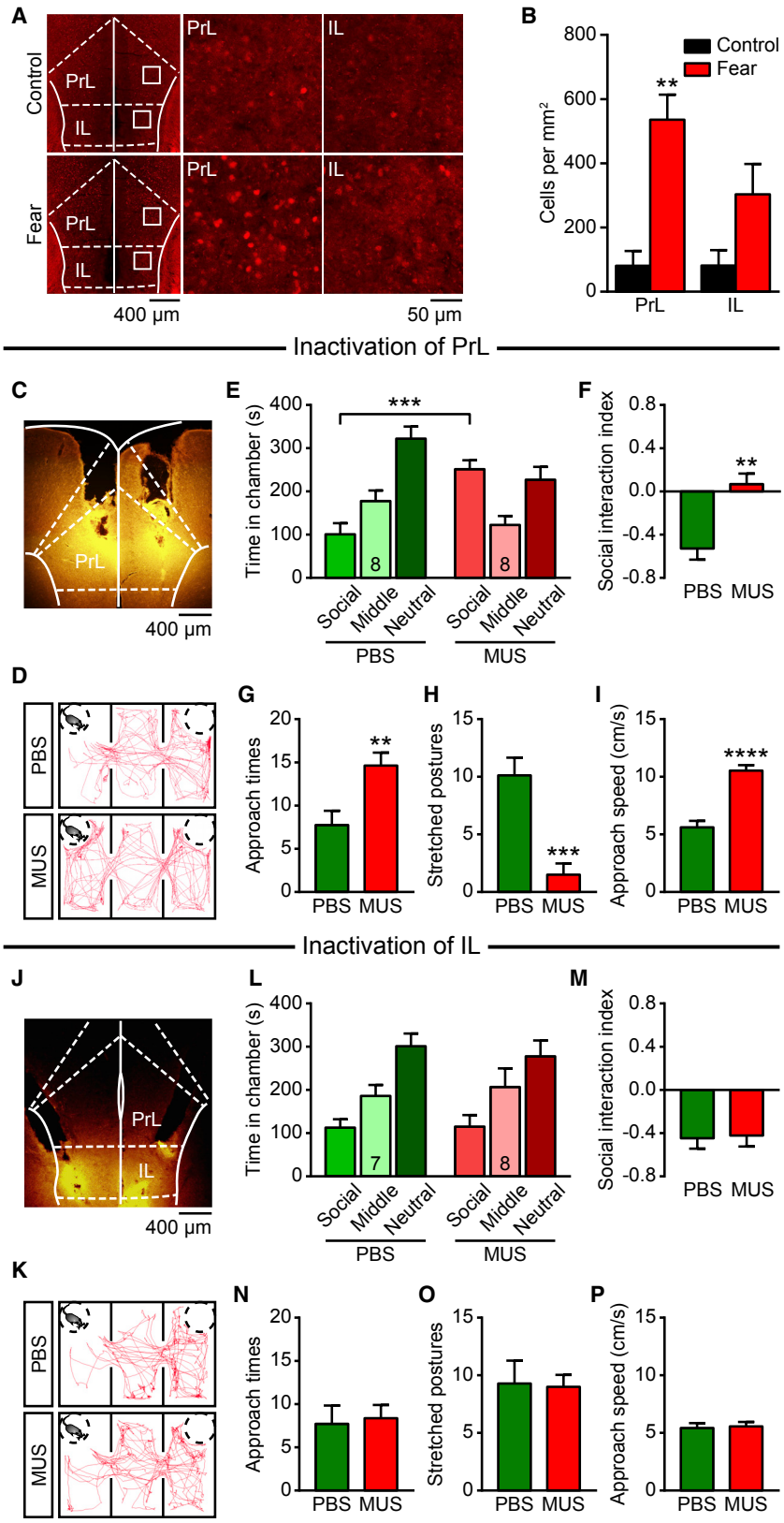

Figure 2. The dmPFC Participates in Conditioned Social Fear Expression

(A) Representative images showing the c-Fos-positive cells in mPFC of two conditioned mice without (top) and with (bottom) social fear expression, respectively. PrL, prelimbic cortex; IL, infralimbic cortex.

(B) Quantification of the number of PrL and IL c-Fos-positive cells of conditioned mice without (black, n = 3 mice) and with (red, n = 3 mice) social fear expression. Error bars indicate mean ± SEM. **p < 0.01; two-way ANOVA, Bonferroni multiple comparison post hoc tests.

(C) Representative micrograph showing the site of fluorescent muscimol (MUS) injection into bilateral dmPFC.

(D) Representative movement traces showing the locations of two social fear conditioned mice injected with either PBS (top) or MUS (bottom) in a three-chamber social interaction test.

(E) Quantification of time spent by PBS-injected and MUS-injected mice in each chamber. Error bars indicate mean ± SEM. ***p < 0.001; two-way ANOVA, Bonferroni multiple comparison post hoc tests. Numbers in columns indicate the number of mice analyzed.

(F) Social interaction index was significantly larger in MUS-injected mice. Error bars indicate mean ± SEM. **p < 0.01; unpaired t test.

(G–I) Quantification of approach times (G), stretched postures (H), and approach speed (I) of PBS-injected and MUS-injected mice upon approaching stimulus mouse. Error bars indicate mean ± SEM. **p < 0.01; ***p < 0.001; ****p < 0.0001; unpaired t test.

(J–P) The same as (C)–(I) but for infralimbic cortex (IL) inactivation.

See also Figures S3–S5.

led to a larger suppression of fear behavior than dmPFC inactivation did. Given the complexity of neuronal circuits underlying fear (Gross and Canteras, 2012; Herry and Johansen, 2014), it is likely that projections from brain regions other than dmPFC to BLA also participate in social fear modulation.

Correlates of dmPFC Neuronal Activity with Social Fear Expression

The dmPFC is a complex circuitry composed of glutamatergic excitatory neurons and GABAergic inhibitory INs. To further explore the dmPFC microcircuitry underlying social fear, we employed chronic electrophysiological recordings (Figure 3A). The well-isolated neurons (241 from 19 conditioned mice; 133 from 8 unconditioned mice) were categorized into narrow-spiking (NS; n = 68, trough to peak duration 239.62 ± 6.57 μs) putative inhibitory INs and wide-spiking (WS; n = 306, trough to peak duration 474.50 ± 2.78 μs) putative pyramidal neurons according to spike features (Figures S6A–S6C) (Kim et al., 2016a, 2016b). The putative inhibitory INs were further classified into fast-spiking parvalbumin (FS-PV) INs (average firing rate >10 Hz) and non-FS NS neurons based on neuronal firing rate (Figure 3B) (Kim et al., 2016b). In a separate cohort of animals, we also used optogenetic tagging method to identify FS-PV INs (Figures S6D–S6G). A total of 19 opto-tagged dmPFC FS-PV INs (10 from 5 conditioned mice; 9 from 5 unconditioned mice) was recorded (Figures 3B, 3F, and 3J).

We then measured the spiking activity of dmPFC neurons during social fear expression, that is, when a conditioned mouse was confronted with a confined stimulus mouse in a social approach test (Figure 3A). During the test, the experimental mice exhibited occasional risk assessment behaviors. In specific, the experimental mice slowly approached the stimulus mouse in a stretched posture and then quickly retreated from the stimulus mouse, indicating an elevated fear state (Figures 1F, 1G, 1L, and 1M; Videos S3 and S4). We therefore focused on the neuronal activities during such risk assessment, the period when experimental mouse was approaching and orientating at the stimulus mouse (Figures 3C and 3E).

We first examined the neuronal activity of WS neuron population. Scatterplot of the mean firing rates of individual WS neurons revealed a mixed modulation (Figure 3D). A subpopulation of WS neurons (42 out of 197, 21%) displayed a sustained firing increase when experimental mice confronted with a social stimulus (Video S3). Only a small proportion of neurons (12 out of 197, 6%) had an inhibitory response upon social risk assessment. The remainder maintained their activity level during fear expression. In comparison, a significantly smaller proportion of pyramidal neurons increased their firing rates upon approaching toward a social target in unconditioned control mice (control: 11%, 12 out of 109 recordings; conditioned: 21%, 42 out of 197 recordings, Fisher's exact test, $p < 0.05$) (Figures 3D and 3H). The hyperactivity of dmPFC pyramidal neurons during social fear expression was further confirmed with a three-chamber testing paradigm (Figure S7).

We next examined the neuronal activity of FS-PV population during social fear expression. Interestingly, in striking contrast to a mixed modulation property observed in WS neurons, the spiking activity declined almost for all FS-PV INs recorded, indicating that social fear expression suppressed FS-PV firing rate (Figure 3E; Video S4). Quantification of the mean discharge rates during social risk assessment confirmed the above observation as 84% of FS-PV INs (27 out of 32, green dots) displayed a significant decrease in firing rate upon social confrontation (Figure 3F). Because response properties were indistinguishable between putative FS-PV INs (n = 22) and opto-tagged FS-PV INs (n = 10), they were pooled for analysis. Instead of a consistent decrease in firing rate of majority of FS-PV INs observed in conditioned mice, the most FS-PV INs maintained their activity levels and a small proportion of neurons (33%, 4 out of 12) even increased their firing rates during social approach in unconditioned control animals (Figures 3I and 3J). Again, the decrease in FS-PV firing upon social approaches in conditioned mice was confirmed with a three-chamber testing paradigm (Figure S7). Therefore, FS-PV INs predominantly decreased their discharge rates upon social fear expression, suggesting a functional role of this IN population during social fear behavior.

Pharmacogenetic Inactivation of dmPFC Principal Neurons Reduces Social Fear

Abnormal hyperactivity of PFC is linked to fear states including social fear (Buff et al., 2016; Kawashima et al., 2016). Consistently, our electrophysiological recordings revealed an elevated firing rate in a subset of dmPFC principal neurons during social fear expression (Figure 3). To know whether the enhanced dmPFC excitability was required for fear expression, we employed a pharmacogenetic approach to inactivate principal neurons during fear expression. Specifically, CaMKIIα-Cre mice (Tsien et al., 1996) were injected bilaterally in dmPFC with a Cre-dependent adeno-associated virus (AAV) expressing mCherry-tagged hM4D, a designer receptor activated exclusively by the otherwise inert agonist clozapine-noxide (CNO) (Armbruster et al., 2007). Immunohistochemistry was used to examine the efficiency and specificity of hM4D expression on CaMKII positive neurons (62.3% ± 8.9% of CaMKII positive neurons expressed hM4D-mCherry; 84.7% ± 2.0% of hM4D-mCherry-expressing neurons were CaMKII positive) (Figure 4A). The relatively low overlaps between CaMKII staining and hM4D-mCherry expression suggest a caveat that this mouse line may not be highly specific for dmPFC excitatory neurons. To verify the effectiveness of pharmacogenetic inactivation, we directly measured the effect of CNO on WS firing *in vivo* in mice implanted with tetrodes. As predicted, the spike rates of WS neurons decreased significantly following CNO administration (baseline: 3.54 ± 0.92 Hz, CNO: 1.83 ± 0.60 Hz; n = 8 neurons from 3 mice; $p < 0.01$; paired t test) (Figure 4B).

Next, we assessed social fear behavior following CNO administration with a three-chamber social interaction test (Figure 4C). As compared to the control CaMKIIα-Cre mice expressing enhanced yellow fluorescent protein (EYFP), those expressing hM4D exhibited a significant increase in the time spent in the social chamber (hM4D: 251.6 ± 46.3 s, n = 8; EYFP: 112.1 ± 26.0 s, n = 10; $p < 0.01$), the social interaction index (hM4D: 0.04 ± 0.17, n = 8; EYFP: −0.49 ± 0.11, n = 10; $p < 0.05$), and times of social approaches (hM4D: 16.1 ± 2.4, n = 8; EYFP: 5.8 ± 1.5, n = 10; $p < 0.01$) (Figures 4D–4F). Furthermore, hM4D mice also exhibited significantly less stretched postures (hM4D: 2.8 ± 1.0,

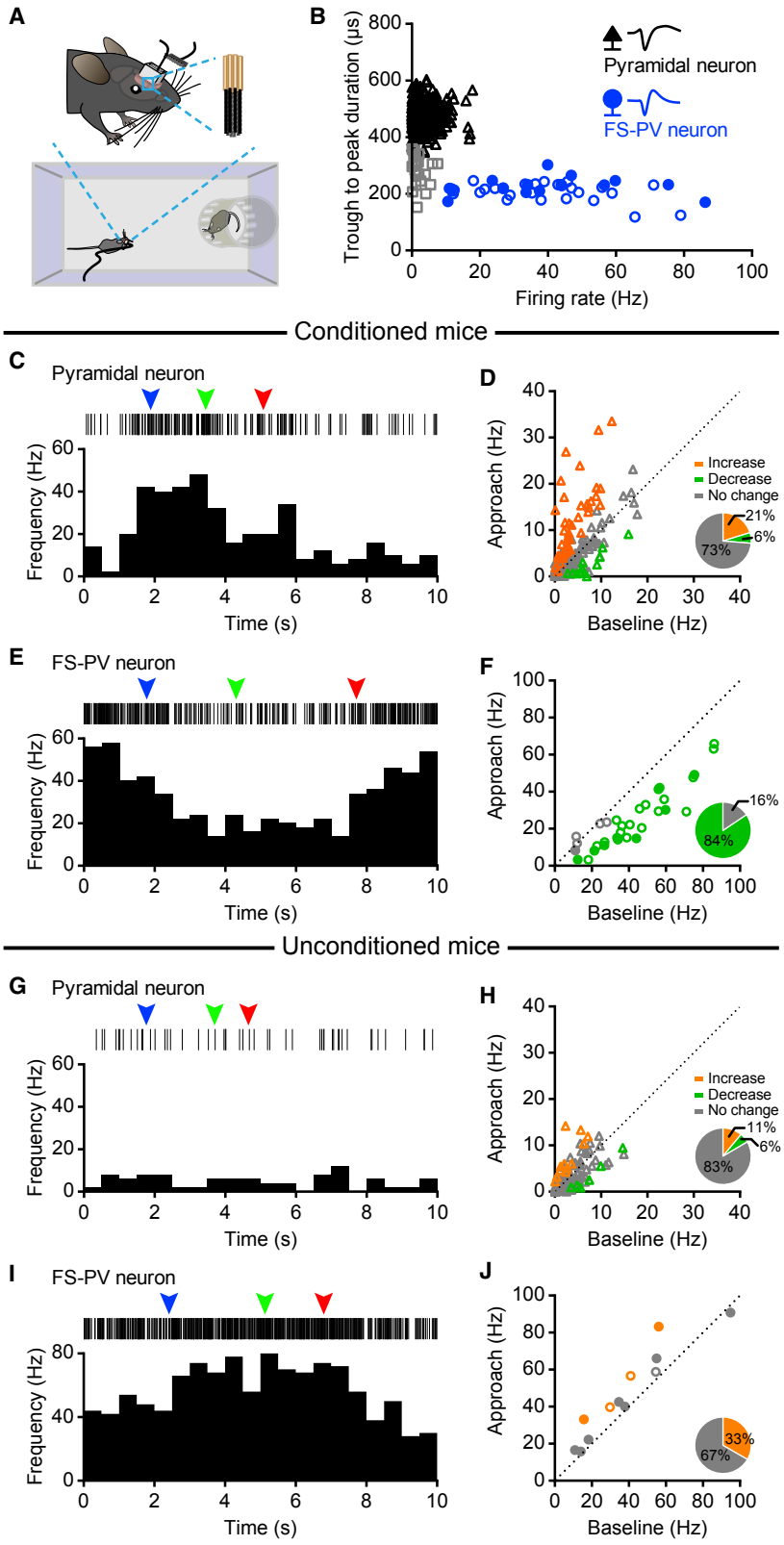

Figure 3. Discharge Profile of dmPFC Pyramidal Cells and FS-PV INs during Social Fear Expression

(A) Schematic illustration of electrophysiological recording from a mouse subjected to a social approach and avoidance test. Enlargement shows multichannel tetrode implantation.

(B) Classification of recorded dmPFC neurons into WS putative pyramidal cells (black triangles), non-FS NS INs (gray squares), and FS-PV INs (blue circles) based on spike waveform and firing rate. Note that filled blue circles represent opto-tagged PV INs. Insets display representative spike waveforms of a WS and an FS-PV, respectively.

(C) Raster plot (top) and peri-stimulus time histogram (PSTH; bottom) of a wide spiking (WS) neuron during the course of a risk assessment. The inverted arrows indicate the onset of approach movement (blue), the most proximity with the stimulus mouse (green), and the retreat from the stimulus mouse (red), respectively.

(D) Correlation of firing rate at baseline and during social risk assessment for individual WS neurons. Orange and green triangles represent individual units with significant higher and lower firing rates during risk assessment, respectively; gray triangles indicate neurons with no significant difference in firing rates. Inset: proportions of WS neurons with significantly increased rates, decreased rates or no change in rates during risk assessment (paired t test).

(E) The same as (C) but for a representative FS-PV INs. Note that the diminished firing rate during social risk assessment.

(F) The same as (D) but for FS-PV population. Note that filled circles represent opto-tagged PV INs.

(G–J) The same as (C)–(F) but for unconditioned control mice.

See also Figures S6 and S7.

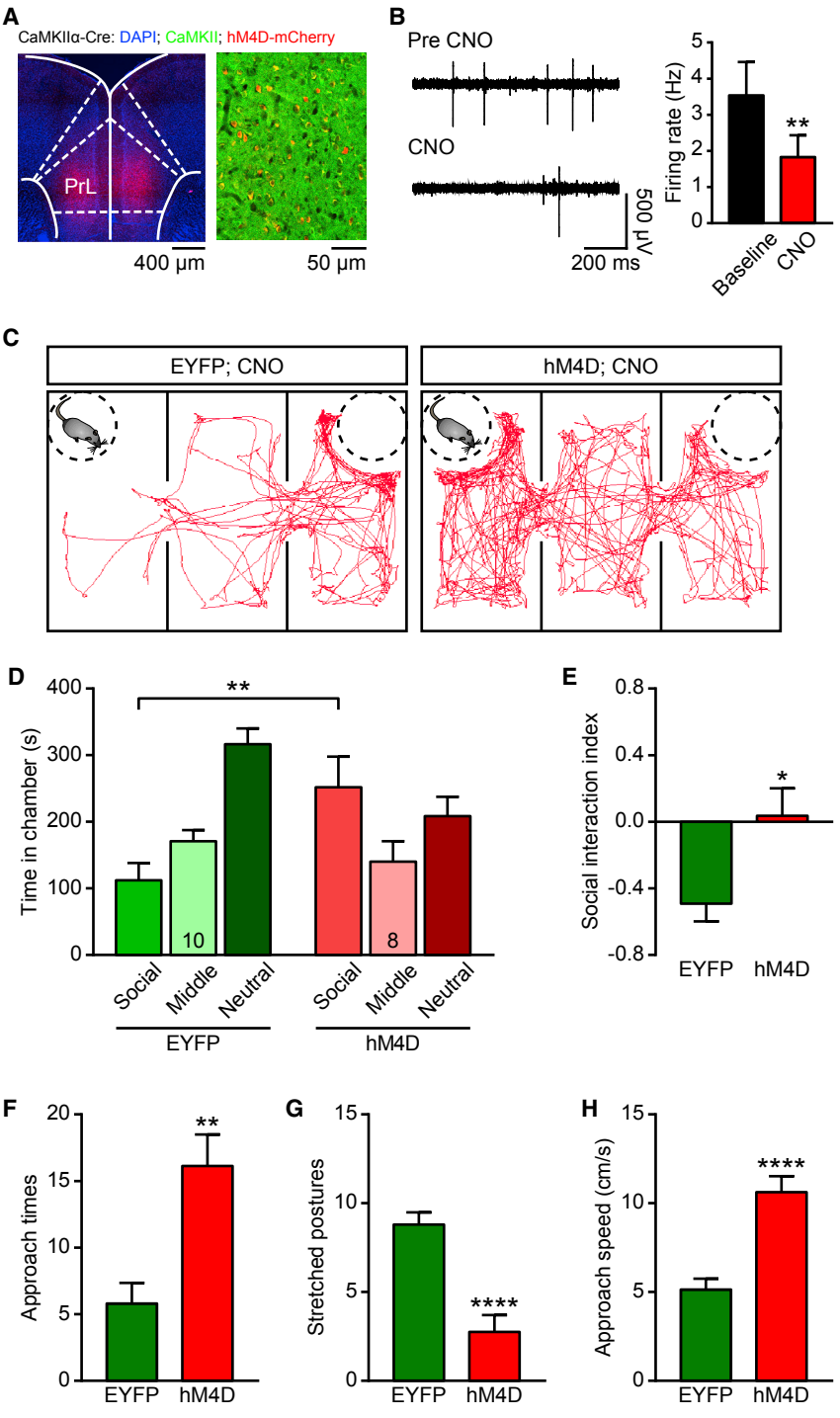

Figure 4. Effect of Pharmacogenetic Inactivation of dmPFC Pyramidal Cells on Social Fear

(A) Location of bilateral viral infection in dmPFC (left) and hM4D expression in CaMKII neurons (right). PrL, prelimbic cortex.

(B) Left: example recording of spontaneous spikes from a WS neuron before (top) and after CNO administration (bottom). Right: statistics of WS firing rates before and after CNO administration. Error bars indicate mean ± SEM (n = 8 neurons from 3 mice).

(C) Representative movement traces showing the locations of an EYFP-expressing control mouse (left) and an hM4D-expressing mouse (right) in a three-chamber test following CNO administration.

(D) Quantification of time spent by EYFP and hM4D mice in each chamber. Note that hM4D mice showed a significant increase in the time spent in the social chamber compared to EYFP mice. Error bars indicate mean ± SEM. **p < 0.01; two-way ANOVA, Bonferroni multiple comparison post hoc tests. Numbers in columns indicate the number of mice analyzed.

(E) Social interaction index was significantly larger in hM4D mice. Error bars indicate mean ± SEM. *p < 0.05; unpaired t test.

(F–H) Quantification of approach times, stretched postures, and approach speed of EYFP and hM4D mice upon approaching stimulus mouse. Error bars indicate mean ± SEM. **p < 0.01; ****p < 0.0001; unpaired t test.

See also Figure S3.

n = 8; EYFP: 8.8 ± 0.7, n = 10; p < 0.0001) and an increased approach speed (hM4D: 10.6 ± 0.9 cm/s, n = 8; EYFP: 5.1 ± 0.6 cm/s, n = 10; p < 0.0001), indicating a direct reduction of fear (Figures 4G and 4H). In a separate experiment, we found that unconditioned control mice spent less time in the social chamber after silencing of CaMKIIα neurons (Figures S3C and S3D). This result raises an alternative possibility that inhibiting dmPFC excitatory neurons could reduce the ability of conditioned mice to express preference for either chamber. However, given that unconditioned control mice still exhibited robust preference for social target even after inactivation of CaMKIIα neurons (time in social chamber: 300.9 ± 10.0 s, n = 8; time in neutral chamber: 168.8 ± 12.4 s, n = 8, p < 0.001; paired t test) (Figures S3C and S3D), this possibility is less likely. Together, these results therefore revealed that suppression of dmPFC principal neurons reduces social fear and hence indicated that their activity is necessary for the top-down control of fear responses.

Pharmacogenetic Activation of dmPFC FS-PV INs Also Reduces Social Fear

Since FS-PV INs form robust functional synapses onto principal neurons, we hypothesized that the reduction of FS neuronal activity increased the firing activity of principal neurons to drive fear behavior in mice. To test this hypothesis, we employed a pharmacogenetic approach to activate FS-PV neurons and examined the consequences of this manipulation on social fear responses. Specifically, we delivered Cre-inducible AAV expressing mCherry-tagged hM3D into the dmPFC of PV-Cre knockin

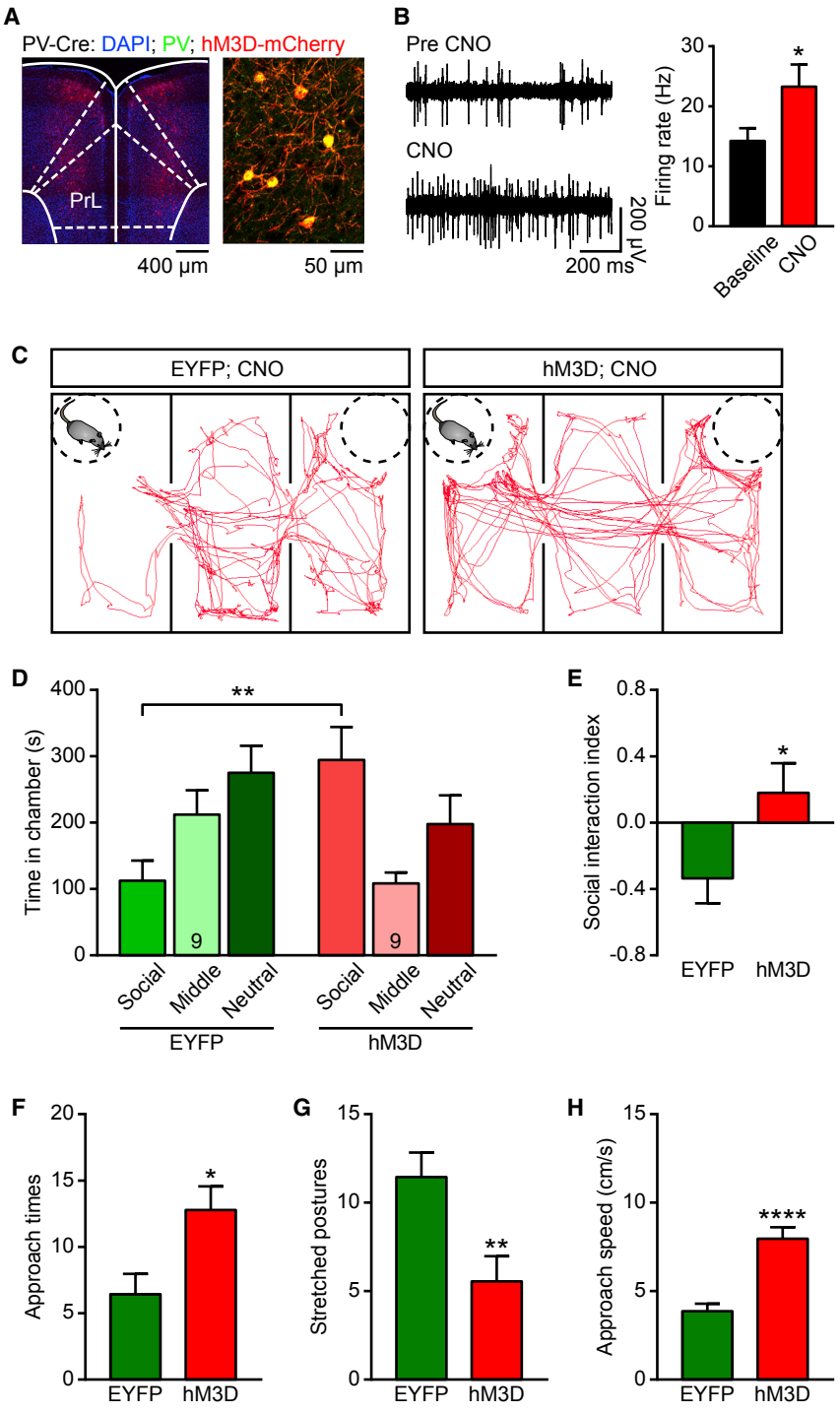

Figure 5. Effect of Pharmacogenetic Activation of dmPFC FS-PV INs on Social Fear

(A) Location of bilateral viral infection in dmPFC (left) and hM3D expression in FS-PV INs (right). PrL, prelimbic cortex.

(B) Left: example recording of spontaneous spikes from an FS-PV neuron before (top) and after CNO administration (bottom). Right: statistics of FS-PV firing rates before and after CNO administration. Error bars indicate mean ± SEM (n = 7 neuron from 4 mice).

(C) Representative movement traces showing the locations of an EYFP-expressing control mouse (left) and an hM3D-expressing mouse (right) in a three-chamber test following CNO administration.

(D) Quantification of time spent by EYFP and hM3D mice in each chamber. Note that hM3D mice showed a significant increase in the time spent in the social chamber compared to EYFP mice. Error bars indicate mean ± SEM. **$p < 0.01$; two-way ANOVA, Bonferroni multiple comparison post hoc tests. Numbers in columns indicate the number of mice analyzed.

(E) Social interaction index was significant larger in hM3D mice. Error bars indicate mean ± SEM. *$p < 0.05$; unpaired t test.

(F–H) Quantification of approach times (F), stretched postures (G), and approach speed (H) of EYFP and hM3D mice upon approaching stimulus mouse. Error bars indicate mean ± SEM. *$p < 0.05$; **$p < 0.01$; ****$p < 0.0001$; unpaired t test.

See also Figures S3 and S8.

mice (Hippenmeyer et al., 2005). Immunohistochemical analysis showed that hM3D expression extensively overlapped with PV INs (87.5% ± 6.9% of PV immunopositive neurons expressed hM3D-mCherry; 89.4% ± 5.4% of hM3D-mCherry-expressing neurons were PV immunopositive), indicating efficient and selective expression of hM3D in FS-PV INs (Figure 5A). To verify the effectiveness of pharmacogenetic activation, we directly measured the effect of CNO on FS-PV firing *in vivo* in mice implanted with tetrodes. As predicted, we observed significantly increased spike rates of FS INs following CNO administration (baseline: 14.22 ± 2.12 Hz, CNO: 23.27 ± 3.69 Hz; n = 7 neurons from 4 mice; $p < 0.05$; paired t test) (Figure 5B).

Next, we assessed social fear behavior following CNO administration with a three-chamber social interaction test (Figure 5C). As compared to the conditioned control PV-Cre mice expressing EYFP, those expressing hM3D exhibited a significant increase in the time spent in the social chamber (hM3D: 294.3 ± 49.8 s, n = 9; EYFP: 112.6 ± 30.1 s, n = 9; $p < 0.01$), the social interaction index (hM3D: 0.18 ± 0.18, n = 9; EYFP: −0.34 ± 0.15, n = 9; $p < 0.05$), and times of social approaches (hM3D: 12.8 ± 1.8, n = 9; EYFP: 6.4 ± 1.5, n = 9; $p < 0.05$) (Figures 5D–5F). Besides, hM3D mice also exhibited significantly less stretched postures (hM3D: 5.6 ± 1.4, n = 9; EYFP: 11.4 ± 1.4, n = 9; $p < 0.01$) and an increased approach speed (hM3D: 8.0 ± 0.7 cm/s, n = 9; EYFP: 3.9 ± 0.4 cm/s, n = 9; $p < 0.0001$), indicating a direct reduction of fear (Figures 5G and 5H). In contrast, in agreement with a recent study

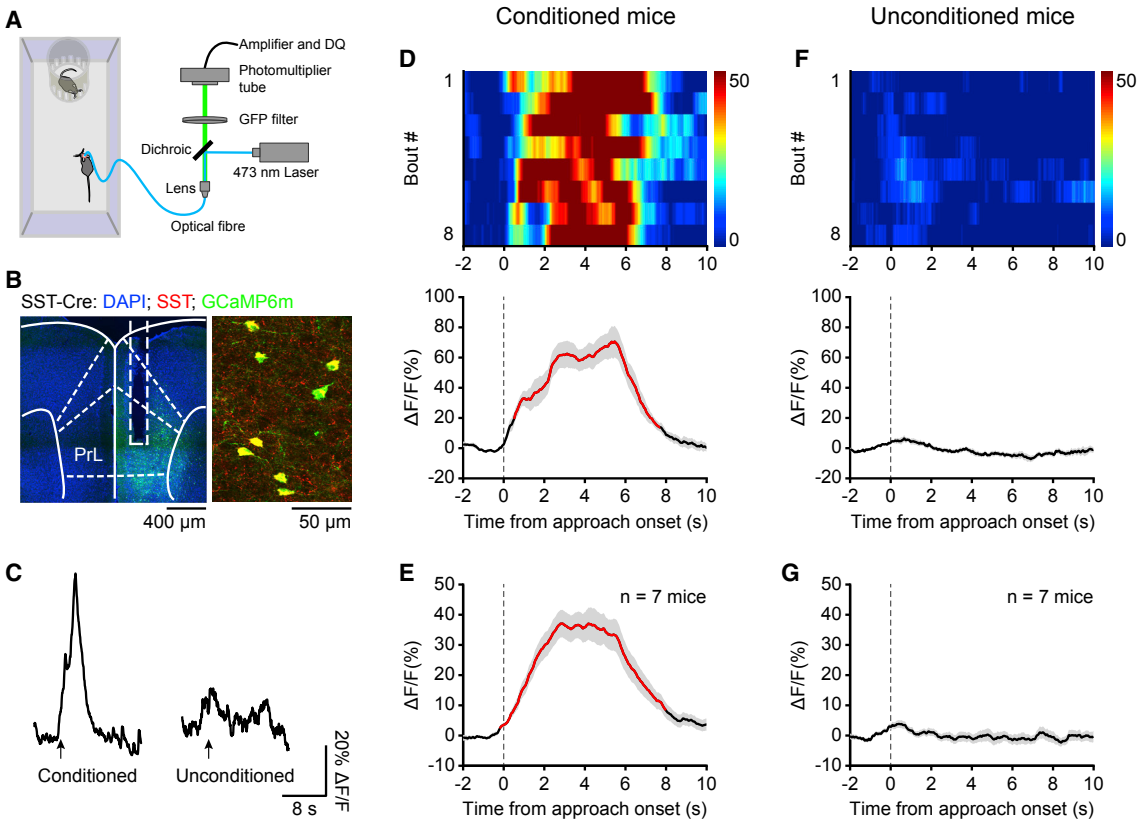

Figure 6. Activity of dmPFC SST INs Is Highly Elevated during Social Fear Expression

(A) Schematic diagram of the fiber photometry setup. Ca^{2+} transients were recorded from GCaMP6m-expressing mPFC SST INs of a SST-Cre mouse subjected to a social approach and avoidance test.

(B) Left: placement of an optic fiber for fiber photometry in dmPFC of a SST-Cre mouse injected with GCaMP6m. Right: GCaMP6m expression in SST INs. PrL, prelimbic cortex.

(C) Representative raw traces of GCaMP6m fluorescence changes associated with social approach of a conditioned mouse (left) and an unconditioned mouse (right), respectively. $\Delta F/F$ represents change in fluorescence from the mean before social approach. Arrows indicate social approach onset.

(D) Ca^{2+} signals associated with social risk assessment during social approach and avoidance test. Upper panel, the heatmap illustration of Ca^{2+} signals aligned to the onset of individual risk assessments. Each row represents one bout, and a total of 8 bouts are illustrated. The color scale at the right indicates $\Delta F/F$. Lower panel, the peri-event plot of the average Ca^{2+} transients. Thick lines indicate mean and shaded areas indicate SEM. Red segments indicate statistically significant increase from the baseline ($p < 0.05$; permutation test).

(E) Mean Ca^{2+} transient associated with risk assessment for the entire test group (n = 7 mice). Thick lines indicate mean and shaded areas indicate SEM. Red segments indicate statistically significant increase from the baseline ($p < 0.05$; permutation test).

(F–G) The same as (D) and (E) but for unconditioned control mice.

See also Figures S9 and S10.

(Ferguson and Gao, 2018), unconditioned control mice spent less time in the social chamber but still exhibited apparent preference for social target after pharmacogenetic activation of PV INs, suggesting that this manipulation neither nonspecifically increased social preference nor interfered with animals' ability to differentiate between regions of their environment (Figures S3E and S3F). Together, these results suggested that activation of FS-PV INs suppressed dmPFC principal neurons and reduced social fear. Consistently, when PV INs were further inactivated with pharmacogenetics, social fear conditioned mice spent even less time in social chamber compared to the conditioned control mice expressing EYFP (Figures S8A–S8C). Therefore, the reduction in firing activity of FS-PV INs plays a pivotal role in gating social fear expression.

Activity of dmPFC SST INs Is Increased during Social Fear Expression

Next, we sought to explore the dmPFC circuit element that provided inhibitory control over FS-PV neurons during fear expression. In mouse neocortex, PV and somatostatin (SST) INs are the two largest populations of GABAergic neurons (Rudy et al., 2011). Also, robust inhibitory synapses from SST neurons onto PV neurons have been observed in both somatosensory and motor cortex (Xu et al., 2013; Zhang et al., 2016). Therefore, we wondered whether it is SST neurons that provided inhibitory control over FS-PV neurons and hence disinhibited dmPFC principal neurons during social fear. To address this issue, we directly measured activities of dmPFC SST neurons with fiber photometry in freely moving mice (Figure 6A). Following stereotaxic

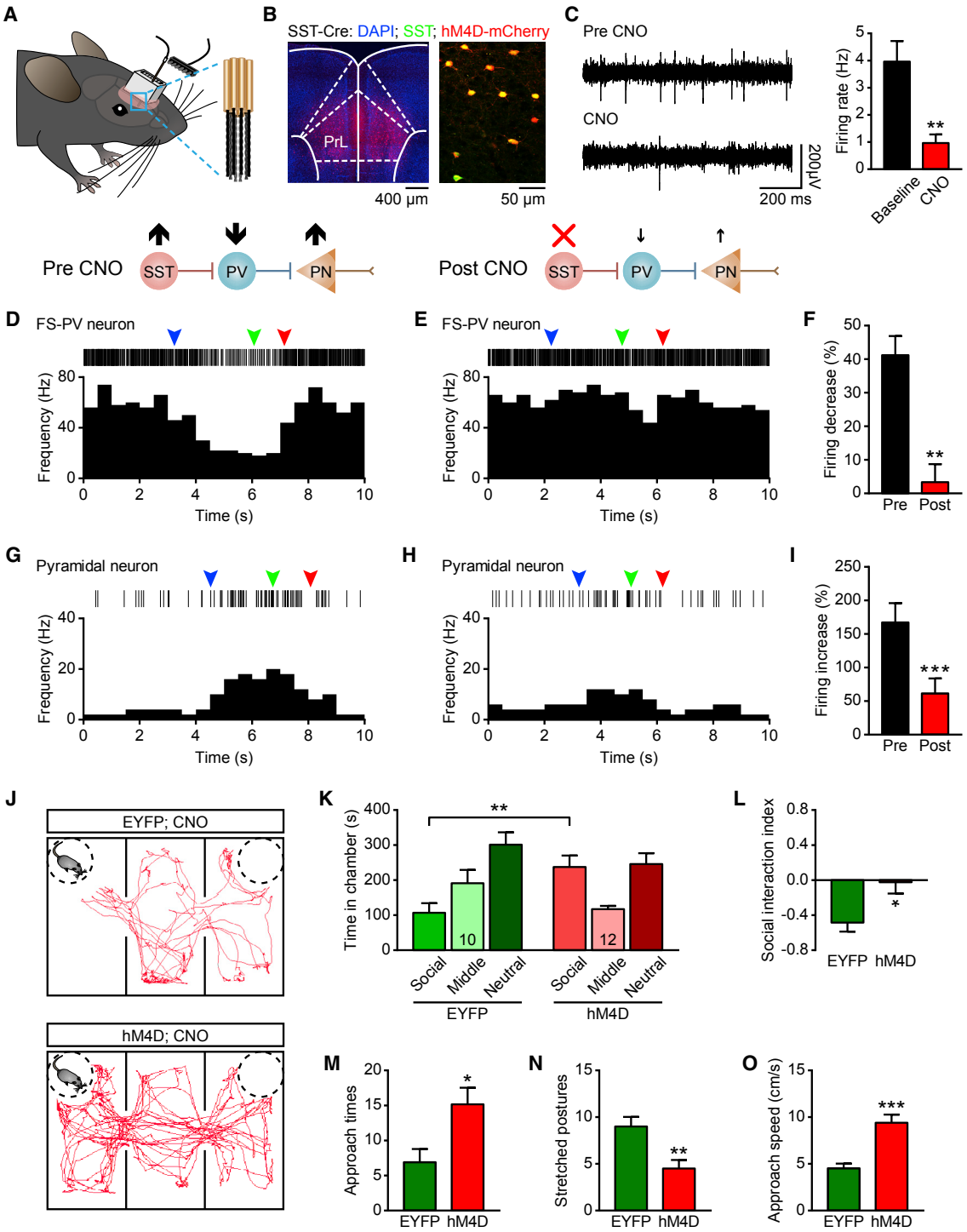

Figure 7. Pharmacogenetic Inactivation of dmPFC SST INs Reduces Social Fear

(A) Schematic illustration of electrophysiological recording from a conditioned mouse. Enlargement shows multichannel tetrode.

(B) Location of bilateral viral infection in dmPFC (left) and hM4D expression in SST INs (right). PrL, prelimbic cortex.

(C) Left: example recording of spontaneous spikes from a putative SST IN before (top) and after CNO administration (bottom). Right: statistics of SST firing rates before and after CNO administration. Error bars indicate mean ± SEM (n = 5 neurons from 3 mice).

(D) Raster plot (top) and peri-stimulus time histogram (PSTH; bottom) of an example FS-PV neuron during the course of a social approach. The inverted arrows indicate the onset of approach movement (blue), the most proximity with the stimulus mouse (green), and the retreat from the stimulus mouse (red), respectively.

(legend continued on next page)

infusion of the Cre-inducible AAV-DIO-GCaMP6m into the dmPFC of SST-Cre knockin mice (Taniguchi et al., 2011), a small optical fiber (230 μm diameter) was implanted for chronic recording of GCaMP fluorescence signals. Histological examination verified the efficiency and specificity of GCaMP expression on SST INs (85.5% ± 2.5% of SST immunopositive neurons expressed GCaMP; 80.6% ± 2.5% of GCaMP-expressing neurons were SST immunopositive) (Figure 6B).

We then measured the Ca^{2+} signals of dmPFC SST INs in mice subjected to a social approach test. There was an increase in GCaMP fluorescence each time when the conditioned mouse approached the stimulus mouse (Figure 6C; Video S5). Also, the increase of fluorescence signals was tightly coupled to the onset of each risk assessment behavior and remained significant throughout the entire risk assessment period until retreat from the stimulus mouse (Figure 6D; Video S5). The average signal peak ($\Delta F/F$) was 38.94% ± 4.49% (mean ± SEM, $p < 0.05$, permutation test, n = 7 mice) (Figure 6E). The increase in calcium signal during social fear expression was further confirmed with a three-chamber testing paradigm (Figure S9). Besides, significantly increased calcium signals were also detected in SST INs of social fear animals acquired with social defeat paradigm (Figures S4I–S4L). However, there was no significant increase in calcium signal (4.36% ± 1.29%, $p > 0.05$, permutation test, n = 7 mice) when control mice approached the stimulus mouse (Figures 6F and 6G). Therefore, dmPFC SST INs were indeed strongly activated by social fear expression.

Since vasoactive intestinal polypeptide (VIP) INs form functional synapses with PV INs and are known to inhibit PV INs to some degree (Pfeffer et al., 2013; Pi et al., 2013), we also examined VIP activities during social fear expression with fiber photometry. In contrast to SST INs, we observed only a negligible increase in fluorescence signals when the conditioned mice approached a stimulus mouse (Figure S10; Video S6). Therefore, under our experimental conditions, dmPFC VIP INs did not seem to be involved in the process of social fear responses.

Together, these results suggest that SST INs are the major circuit elements that provide robust inhibition to dmPFC FS-PV INs during social fear expression.

Pharmacogenetic Inactivation of SST INs Alleviates Social Fear

To determine whether the increased firing activity of SST INs is necessary to suppress FS-PV INs and to drive social fear, we employed a pharmacogenetic approach to inactivate SST INs and examined its consequence on activities of pyramidal cells and FS-PV INs and also mouse social fear behavior. For this purpose, a Cre-dependent hM4D virus was bilaterally targeted to dmPFC of SST-Cre mice. Immunohistochemical examination verified the efficiency and specificity of hM4D expression on SST INs (83.3% ± 5.0% of SST immunopositive neurons expressed hM4D-mCherry; 93.8% ± 6.1% of hM4D-mCherry-expressing neurons were SST immunopositive) (Figure 7B). To verify the effectiveness of pharmacogenetic inactivation, we directly measured the effect of CNO on neuronal firing *in vivo* in mice implanted with tetrodes. We observed that the firing rates of a subset of neurons, putative SST INs, decreased significantly following CNO administration (baseline: 3.96 ± 0.76 Hz, CNO: 0.96 ± 0.32 Hz; n = 5 neurons from 3 mice; $p < 0.01$; paired t test) (Figures 7A and 7C). As anticipated, following SST inactivation, the firing rate decrease in FS-PV neurons upon approaching a social target was largely suppressed (pre: 41.17% ± 5.71%; post: 3.35% ± 5.36%; n = 5; $p < 0.01$) (Figures 7D–7F). Accordingly, for the pyramidal cells showing increased spiking activities during social approach, the firing rate increase was significantly reduced after SST inactivation (pre: 167.27% ± 28.73%; post: 61.46% ± 22.41%; n = 10; $p < 0.001$) (Figures 7G–7I). These data demonstrate that SST activity inhibits FS-PV neurons and hence enhances pyramidal output. SST inactivation thus suppressed this disinhibitory circuit and pyramidal cells therefore became less active.

Next, we assessed social fear behavior following CNO administration with a three-chamber social interaction test (Figure 7J). As compared to the conditioned control SST-Cre mice expressing EYFP, those expressing hM4D exhibited a significant increase in the time spent in the social chamber (hM4D: 237.1 ± 33.2 s, n = 12; EYFP: 106.9 ± 27.2 s, n = 10; $p < 0.01$), the social interaction index (hM4D: −0.02 ± 0.13, n = 12; EYFP: −0.48 ± 0.10, n = 10; $p < 0.05$), and times of social approaches (hM4D: 15.2 ± 2.4, n = 12; EYFP: 6.9 ± 1.9, n = 10; $p < 0.05$) (Figures 7K–7M). Moreover, hM4D mice also exhibited significantly less stretched postures (hM4D: 4.5 ± 0.9, n = 12; EYFP: 9.0 ± 1.0, n = 10; $p < 0.01$) and an increased approach speed (hM4D: 9.4 ± 0.9 cm/s, n = 12; EYFP: 4.5 ± 0.5 cm/s, n = 10; $p < 0.001$), indicating a direct reduction of fear (Figures 7N and 7O). Similarly, when SST INs were inactivated with pharmacogenetics, significantly reduced social avoidance was observed in animals acquired with social defeat paradigm (Figures S4M and S4N). In contrast, inactivation of SST INs did not alter the time spent in the social chamber in unconditioned control mice, suggesting that this manipulation neither nonspecifically

(E) The same as (D) but at an hour after CNO administration. Note that following SST inactivation, the FS-PV firing rate decrease upon social approach was largely suppressed.
(F) Statistics of FS-PV firing rate decrease before and after CNO administration. Error bars indicate mean ± SEM n = 5, **$p < 0.01$; paired t test.
(G–I) The same as (D)–(F) but for pyramidal neurons. n = 10, ***$p < 0.001$; paired t test.
(J) Representative movement traces showing the locations of an EYFP-expressing control mouse (top) and an hM4D-expressing mouse (bottom) in a three-chamber test following CNO administration.
(K) Quantification of time spent by EYFP and hM4D mice in each chamber. Error bars indicate mean ± SEM. **$p < 0.01$; two-way ANOVA, Bonferroni multiple comparison post hoc tests. Numbers in columns indicate the number of mice analyzed.
(L) Social interaction index was significant larger in hM4D mice. Error bars indicate mean ± SEM. *$p < 0.05$; unpaired t test.
(M–O) Quantification of approach times, stretched postures, and approach speed of EYFP and hM4D mice upon approaching stimulus mouse. Error bars indicate mean ± SEM. *$p < 0.05$; **$p < 0.01$; ***$p < 0.001$; unpaired t test.
See also Figures S3 and S8.

increased social preference nor interfered with animals' ability to differentiate between regions of their environment (Figures S3G and S3H). Together, these results suggested that inactivation of dmPFC SST INs reinstated PV-mediated inhibition onto principal neurons and hence reduced social fear. Consistently, when SST INs were further activated with pharmacogenetics, social fear conditioned mice spent even less time in social chamber compared to the conditioned control mice expressing EYFP (Figures S8D–S8F). Therefore, the elevated activity of SST INs suppressed PV INs and disinhibited pyramidal cells and consequently enhanced dmPFC output to drive social fear responses.

DISCUSSION

An Animal Model of SAD Induced by SFC

Despite its prevalence and disabling consequences, the underlying neurobiology of SAD remained largely unknown. The reason is in part due to the fact that there was no appropriate animal model for SAD. Previously, social defeat and foot-shock exposure, among others, are the most commonly used paradigms that could recapitulate core behavioral symptoms of SAD in rodents (Toth and Neumann, 2013). However, none of these paradigms induced behavioral alterations specifically in the social domain, as impairments in general anxiety and locomotion and also depressive-like phenotypes were observed in experimental animals as well (Denmark et al., 2010; Hollis et al., 2010).

To study the neural mechanism underlying social fear precisely, it is crucial to develop specific animal models. As a major advance, Toth et al. (2012) recently developed a SFC paradigm, which is able to induce social fear in rodents without accompanying impairments in other behavioral measures. The conditioning paradigm employed in the present study is in principle adopted from the one proposed by Toth et al. (2012) but with several significant modifications (see STAR Methods for detail). Besides, to avoid context-dependent fear expression, all social behavior examinations were conducted in a novel environment but not in the conditioning chamber (Figure 1). The observed fear behavioral manifestations here thus reflect the emotional state specifically provoked by social stimulus.

Our modified SFC paradigm efficiently induced robust and long-lasting social fear to conspecifics of either gender, but not to nonsocial stimulus such as a novel object (Figures 1 and S1). More importantly, in agreement with previous reports (Toth et al., 2012), animals that underwent SFC did not show confounding behavioral alterations in nonsocial domains (Figure S2). Therefore, it represents an appropriate animal paradigm to study the neural foundations underlying social fear.

Prefrontal Disinhibitory Microcircuit Underlying Social Fear Expression

Both human and animal studies have revealed that prefrontal hyperactivity is causally linked to fear expression (Buff et al., 2016; Burgos-Robles et al., 2009; Kawashima et al., 2016). Cortical network activity is under tight control of a variety of GABAergic inhibitory neurons (Isaacson and Scanziani, 2011; Tremblay et al., 2016; Xu et al., 2013). By using an auditory fear conditioning paradigm, Courtin et al. recently demonstrate that dmPFC hyperactivity is due to a diminished activity of PV INs during fear expression (Courtin et al., 2014). However, the circuit elements that provide inhibitory control over PV INs activity were not known.

In our conditioning paradigm, the experimental mouse was free from foot shock when it was away from the social target and got foot shock only when approaching and interacting with the stimulus mouse. Consequently, during social fear expression tests, the conditioned mice approached the stimulus mouse at a slow speed in stretched postures, behavioral indicators of an elevated fear state in rodents that was not observed in unconditioned control animals (Figure 1) (Toth et al., 2012). Accordingly, we examined the neuronal activities when experimental mouse was approaching and orientating at the stimulus mouse. Our data corroborated previous findings by showing that PV INs firing rate was significantly suppressed during social fear expression (Figure 3). The reduction in PV firing is responsible for the elevation of principle neurons' firing and hence the social fear since either phamacogenetic activation of PV INs or inactivation of pyramidal cells largely reversed fear behavior (Figures 4 and 5). More importantly, we further revealed that it is SST INs that inhibited PV INs based on three lines of evidence. First, there was a robust elevation in neuronal activity of SST INs during social fear expression (Figure 6). Second, when SST INs were pharmacogenetically inactivated, the firing rate decrease in FS-PV neurons upon social approach was largely suppressed (Figure 7). Third, the degree of social fear in conditioned mice was significantly reduced following SST INs inactivation (Figure 7).

An elegant study by Yizhar et al. (2011) demonstrates that elevation in prefrontal excitation/inhibition (E/I) balance by raising pyramidal neurons' activity reduces social interaction, whereas compensatory activation of PV neurons partially rescues social impairments. Our study is different from the one by Yizhar et al. (2011) in terms of the animals' emotional state. Yizhar et al. (2011) examines normal social interaction in naive animals, yet ours investigates abnormal social interaction in animals with conditioned social fear. In the present study, phamacogenetic inactivation of pyramidal cells or activation of PV neurons not only increased social investigation, but also reduced stretched postures and increased approach times and approach speed (Figures 4 and 5). These behavioral alterations indicate a direct reduction of fear in conditioned animals. Therefore, inactivation of pyramidal cells or activation of PV neurons indeed acts to reduce social fear expression in conditioned mice.

Changes in network activity and animal social behavior are essentially determined by alterations in neuronal circuits (Allsop et al., 2018; Franklin et al., 2017; Zelikowsky et al., 2018). Our data demonstrate that neuronal activities of dmPFC inhibitory neurons were potently modified by aversive social experience. As compared to naive mice, activity of SST INs of conditioned mice dramatically increased when confronted with a conspecific (Figure 6). However, as a striking contrast, we did not see a noticeable change in neuronal activity of VIP INs (Figure S10), although both SST INs and VIP INs form functional synapses with PV INs (Pfeffer et al., 2013; Pi et al., 2013; Xu et al., 2013; Zhang et al., 2016). In other words, SFC-induced neuronal

plasticity occurred in a cell-type-specific manner. As a consequence, the heightened activity of SST INs but not VIP INs inhibited PV INs and hence disinhibited dmPFC principle cells to drive social fear responses.

The conditioning stimulus (i.e., a conspecific mouse) to induce social fear in our study likely represents a combination of sensory inputs from multiple modalities including olfaction, vision, and audition. Given that PFC is a higher-order cortical area that integrates incoming information from multiple sensory modalities, the prefrontal circuit mechanism revealed for social fear could be applicable to conditioned fear acquired with sensory stimulus from a single modality. Indeed, when foot shock was paired with minty, the experimental mice developed avoidance to minty after conditioning, and the Ca^{2+} signals of SST INs increased when conditioned mice approached the minty during fear expression (Figure S11). Moreover, following SST INs inactivation with pharmacogenetics, conditioned mice showed significantly less avoidance to minty (Figure S11). Therefore, dmPFC manipulation, that is SST INs inactivation, also reduced conditioned fear expression to minty. However, given that information flow from different sensory modalities enters dmPFC at different routes, it is possible that the neuronal circuits upstream of dmPFC could differ.

How are SST INs recruited during social fear expression? PFC receives various inputs from both cortical and subcortical brain regions. Although the precise driving force for SST INs during social fear expression is to be determined, one possibility points to neuromodulatory inputs, particularly cholinergic input originated in basal forebrain and noradrenergic input from locus coeruleus of the brain stem based on the following observations. First of all, both cholinergic and noradrenergic nuclei send dense projections to PFC (Chandler and Waterhouse, 2012). Second, SST INs are potently activated by either acetylcholine (Kawaguchi, 1997; Xu et al., 2013) or noradrenaline (Kawaguchi and Shindou, 1998). Last but not the least, both cholinergic neurons in basal forebrain and noradrenergic neurons in locus coeruleus are previously shown to participate in fear expression (Gozzi et al., 2010; Soya et al., 2017). The disinhibition of principle neurons as a result of cholinergic and/or noradrenergic activation of SST INs may work in concert with their direct activation of principle neurons (Grzelka et al., 2017; Hedrick and Waters, 2015) to reinforce dmPFC output to drive fear expression.

The dmPFC principal neurons provide final output to downstream brain structures for top-down behavioral controls. Anatomically, the dmPFC principal neurons target multiple cortical and subcortical brain structures. Some of these targets, such as the amygdala (Ciocchi et al., 2010; Haubensak et al., 2010; LeDoux, 2000; Likhtik et al., 2014), the periaqueductal gray (PAG) (Franklin et al., 2017; Rozeske et al., 2018), and the paraventricular nucleus of the thalamus (PVT) (Do-Monte et al., 2015; Penzo et al., 2015) are known to be involved in various forms of fear and anxiety regulation. Social fear could share the same downstream targets as amygdala, PAG and PVT, or alternatively it could possess different targets given the specificity of social stimuli. Nevertheless, the exact target(s) of dmPFC outputs in the control of social fear behavior are to be investigated in future studies.

STAR★METHODS

Detailed methods are provided in the online version of this paper and include the following:

- KEY RESOURCES TABLE
- CONTACT FOR REAGENT AND RESOURCE SHARING
- EXPERIMENTAL MODEL AND SUBJECT DETAILS
- METHOD DETAILS
  - Social Fear Conditioning Paradigm
  - Three-Chamber Social Interaction Test
  - Social Preference-Avoidance Test
  - Open Field Test
  - Forced Swim Test
  - Social Defeat Paradigm and Social Fear Test
  - Drug Infusion
  - Virus Injection
  - Surgical Implantation of Tetrodes
  - Optogenetic Tagging of PV INs
  - Electrophysiological Data Acquisition during Social Fear Expression
  - Spike Sorting
  - Unit Classification and Firing Rate Analysis
  - Neuronal Responses to Pharmacogenetic Manipulations
  - Fiber Photometry
  - Pharmacogenetic Inactivation during Behavior
  - Immunohistochemistry
- QUANTIFICATION AND STATISTICAL ANALYSIS

SUPPLEMENTAL INFORMATION

Supplemental Information can be found with this article online at https://doi.org/10.1016/j.neuron.2019.02.026.

ACKNOWLEDGMENTS

We thank David Anderson, Edvard Moser, and Minmin Luo for scientific discussions and the anonymous reviewers for their valuable comments and suggestions. We thank Z. Josh Huang for SST-Cre and VIP-Cre mice. We thank Wang Xi, Zhiguo Shi, and Mingli Song for help with electrophysiological recording and data analysis, and Core Facilities of Zhejiang University Institute of Neuroscience. This research was supported by grants from the National Key R&D Program of China (2016YFA0501000), the National Natural Science Foundation of China (31471025, 91432110), the Zhejiang Provincial Natural Science Foundation of China (LR17H090002), the Chinese Ministry of Education Project 111 Program (B13026), and the Non-profit Central Research Institute Fund of Chinese Academy of Medical Sciences (2017PT31038 and 2018PT31041) to Han Xu.

AUTHOR CONTRIBUTIONS

Haifeng Xu, L.L., Y.T., and J.W. performed most of the experiments and data analysis. J.L. and H.Z. conducted immunohistochemistry experiments. J.Z. did social defeat experiments. M.H., T.-L.X., and S.D. provided resources and commented on the manuscript. H.X. supervised the project and wrote the manuscript with the help from all contributing authors.

DECLARATION OF INTERESTS

The authors declare no competing interests.

Received: June 11, 2018
Revised: November 18, 2018
Accepted: February 15, 2019
Published: March 18, 2019

REFERENCES

Allsop, S.A., Wichmann, R., Mills, F., Burgos-Robles, A., Chang, C.J., Felix-Ortiz, A.C., Vienne, A., Beyeler, A., Izadmehr, E.M., Glober, G., et al. (2018). Corticoamygdala Transfer of Socially Derived Information Gates Observational Learning. Cell *173*, 1329–1342.e18.

American Psychiatric Association (2013). Diagnostic and Statistical Manual of Mental Disorders (DSM-5) (American Psychiatric Pub).

Armbruster, B.N., Li, X., Pausch, M.H., Herlitze, S., and Roth, B.L. (2007). Evolving the lock to fit the key to create a family of G protein-coupled receptors potently activated by an inert ligand. Proc. Natl. Acad. Sci. USA *104*, 5163–5168.

Ascoli, G.A., Alonso-Nanclares, L., Anderson, S.A., Barrionuevo, G., Benavides-Piccione, R., Burkhalter, A., Buzsáki, G., Cauli, B., Defelipe, J., Fairén, A., et al.; Petilla Interneuron Nomenclature Group (2008). Petilla terminology: nomenclature of features of GABAergic interneurons of the cerebral cortex. Nat. Rev. Neurosci. *9*, 557–568.

Buff, C., Brinkmann, L., Neumeister, P., Feldker, K., Heitmann, C., Gathmann, B., Andor, T., and Straube, T. (2016). Specifically altered brain responses to threat in generalized anxiety disorder relative to social anxiety disorder and panic disorder. Neuroimage Clin. *12*, 698–706.

Burgos-Robles, A., Vidal-Gonzalez, I., and Quirk, G.J. (2009). Sustained conditioned responses in prelimbic prefrontal neurons are correlated with fear expression and extinction failure. J. Neurosci. *29*, 8474–8482.

Cardin, J.A., Carlén, M., Meletis, K., Knoblich, U., Zhang, F., Deisseroth, K., Tsai, L.H., and Moore, C.I. (2009). Driving fast-spiking cells induces gamma rhythm and controls sensory responses. Nature *459*, 663–667.

Chandler, D., and Waterhouse, B.D. (2012). Evidence for broad versus segregated projections from cholinergic and noradrenergic nuclei to functionally and anatomically discrete subregions of prefrontal cortex. Front. Behav. Neurosci. *6*, 20.

Ciocchi, S., Herry, C., Grenier, F., Wolff, S.B., Letzkus, J.J., Vlachos, I., Ehrlich, I., Sprengel, R., Deisseroth, K., Stadler, M.B., et al. (2010). Encoding of conditioned fear in central amygdala inhibitory circuits. Nature *468*, 277–282.

Courtin, J., Chaudun, F., Rozeske, R.R., Karalis, N., Gonzalez-Campo, C., Wurtz, H., Abdi, A., Baufreton, J., Bienvenu, T.C., and Herry, C. (2014). Prefrontal parvalbumin interneurons shape neuronal activity to drive fear expression. Nature *505*, 92–96.

Denmark, A., Tien, D., Wong, K., Chung, A., Cachat, J., Goodspeed, J., Grimes, C., Elegante, M., Suciu, C., Elkhayat, S., et al. (2010). The effects of chronic social defeat stress on mouse self-grooming behavior and its patterning. Behav. Brain Res. *208*, 553–559.

Do-Monte, F.H., Quiñones-Laracuente, K., and Quirk, G.J. (2015). A temporal shift in the circuits mediating retrieval of fear memory. Nature *519*, 460–463.

Etkin, A., Egner, T., and Kalisch, R. (2011). Emotional processing in anterior cingulate and medial prefrontal cortex. Trends Cogn. Sci. *15*, 85–93.

Ferguson, B.R., and Gao, W.J. (2018). Thalamic Control of Cognition and Social Behavior Via Regulation of Gamma-Aminobutyric Acidergic Signaling and Excitation/Inhibition Balance in the Medial Prefrontal Cortex. Biol. Psychiatry *83*, 657–669.

Fishell, G., and Rudy, B. (2011). Mechanisms of inhibition within the telencephalon: "where the wild things are". Annu. Rev. Neurosci. *34*, 535–567.

Franklin, T.B., Silva, B.A., Perova, Z., Marrone, L., Masferrer, M.E., Zhan, Y., Kaplan, A., Greetham, L., Verrechia, V., Halman, A., et al. (2017). Prefrontal cortical control of a brainstem social behavior circuit. Nat. Neurosci. *20*, 260–270.

Golden, S.A., Covington, H.E., 3rd, Berton, O., and Russo, S.J. (2011). A standardized protocol for repeated social defeat stress in mice. Nat. Protoc. *6*, 1183–1191.

Gozzi, A., Jain, A., Giovannelli, A., Bertollini, C., Crestan, V., Schwarz, A.J., Tsetsenis, T., Ragozzino, D., Gross, C.T., and Bifone, A. (2010). A neural switch for active and passive fear. Neuron *67*, 656–666.

Gross, C.T., and Canteras, N.S. (2012). The many paths to fear. Nat. Rev. Neurosci. *13*, 651–658.

Grzelka, K., Kurowski, P., Gawlak, M., and Szulczyk, P. (2017). Noradrenaline Modulates the Membrane Potential and Holding Current of Medial Prefrontal Cortex Pyramidal Neurons via β_1-Adrenergic Receptors and HCN Channels. Front. Cell. Neurosci. *11*, 341.

Haubensak, W., Kunwar, P.S., Cai, H., Ciocchi, S., Wall, N.R., Ponnusamy, R., Biag, J., Dong, H.W., Deisseroth, K., Callaway, E.M., et al. (2010). Genetic dissection of an amygdala microcircuit that gates conditioned fear. Nature *468*, 270–276.

Hedrick, T., and Waters, J. (2015). Acetylcholine excites neocortical pyramidal neurons via nicotinic receptors. J. Neurophysiol. *113*, 2195–2209.

Herry, C., and Johansen, J.P. (2014). Encoding of fear learning and memory in distributed neuronal circuits. Nat. Neurosci. *17*, 1644–1654.

Hippenmeyer, S., Vrieseling, E., Sigrist, M., Portmann, T., Laengle, C., Ladle, D.R., and Arber, S. (2005). A developmental switch in the response of DRG neurons to ETS transcription factor signaling. PLoS Biol. *3*, 878–890.

Hollis, F., Wang, H., Dietz, D., Gunjan, A., and Kabbaj, M. (2010). The effects of repeated social defeat on long-term depressive-like behavior and short-term histone modifications in the hippocampus in male Sprague-Dawley rats. Psychopharmacology (Berl.) *211*, 69–77.

Isaacson, J.S., and Scanziani, M. (2011). How inhibition shapes cortical activity. Neuron *72*, 231–243.

Kamigaki, T., and Dan, Y. (2017). Delay activity of specific prefrontal interneuron subtypes modulates memory-guided behavior. Nat. Neurosci. *20*, 854–863.

Karalis, N., Dejean, C., Chaudun, F., Khoder, S., Rozeske, R.R., Wurtz, H., Bagur, S., Benchenane, K., Sirota, A., Courtin, J., and Herry, C. (2016). 4-Hz oscillations synchronize prefrontal-amygdala circuits during fear behavior. Nat. Neurosci. *19*, 605–612.

Kawaguchi, Y. (1997). Selective cholinergic modulation of cortical GABAergic cell subtypes. J. Neurophysiol. *78*, 1743–1747.

Kawaguchi, Y., and Shindou, T. (1998). Noradrenergic excitation and inhibition of GABAergic cell types in rat frontal cortex. J. Neurosci. *18*, 6963–6976.

Kawashima, C., Tanaka, Y., Inoue, A., Nakanishi, M., Okamoto, K., Maruyama, Y., Oshita, H., Ishitobi, Y., Aizawa, S., Masuda, K., et al. (2016). Hyperfunction of left lateral prefrontal cortex and automatic thoughts in social anxiety disorder: A near-infrared spectroscopy study. J. Affect. Disord. *206*, 256–260.

Kim, D., Jeong, H., Lee, J., Ghim, J.W., Her, E.S., Lee, S.H., and Jung, M.W. (2016a). Distinct Roles of Parvalbumin- and Somatostatin-Expressing Interneurons in Working Memory. Neuron *92*, 902–915.

Kim, H., Ährlund-Richter, S., Wang, X., Deisseroth, K., and Carlén, M. (2016b). Prefrontal Parvalbumin Neurons in Control of Attention. Cell *164*, 208–218.

Kvitsiani, D., Ranade, S., Hangya, B., Taniguchi, H., Huang, J.Z., and Kepecs, A. (2013). Distinct behavioural and network correlates of two interneuron types in prefrontal cortex. Nature *498*, 363–366.

LeDoux, J.E. (2000). Emotion circuits in the brain. Annu. Rev. Neurosci. *23*, 155–184.

Lee, S.H., Kwan, A.C., Zhang, S., Phoumthipphavong, V., Flannery, J.G., Masmanidis, S.C., Taniguchi, H., Huang, Z.J., Zhang, F., Boyden, E.S., et al. (2012). Activation of specific interneurons improves V1 feature selectivity and visual perception. Nature *488*, 379–383.

Lee, S., Kruglikov, I., Huang, Z.J., Fishell, G., and Rudy, B. (2013). A disinhibitory circuit mediates motor integration in the somatosensory cortex. Nat. Neurosci. *16*, 1662–1670.

Likhtik, E., Stujenske, J.M., Topiwala, M.A., Harris, A.Z., and Gordon, J.A. (2014). Prefrontal entrainment of amygdala activity signals safety in learned fear and innate anxiety. Nat. Neurosci. *17*, 106–113.

Lungwitz, E.A., Stuber, G.D., Johnson, P.L., Dietrich, A.D., Schartz, N., Hanrahan, B., Shekhar, A., and Truitt, W.A. (2014). The role of the medial prefrontal cortex in regulating social familiarity-induced anxiolysis. Neuropsychopharmacology *39*, 1009–1019.

Menon, R., Grund, T., Zoicas, I., Althammer, F., Fiedler, D., Biermeier, V., Bosch, O.J., Hiraoka, Y., Nishimori, K., Eliava, M., et al. (2018). Oxytocin Signaling in the Lateral Septum Prevents Social Fear during Lactation. Curr. Biol. *28*, 1066–1078.e6.

Miao, C., Cao, Q., Moser, M.B., and Moser, E.I. (2017). Parvalbumin and Somatostatin Interneurons Control Different Space-Coding Networks in the Medial Entorhinal Cortex. Cell *171*, 507–521.e17.

Moy, S.S., Nadler, J.J., Perez, A., Barbaro, R.P., Johns, J.M., Magnuson, T.R., Piven, J., and Crawley, J.N. (2004). Sociability and preference for social novelty in five inbred strains: an approach to assess autistic-like behavior in mice. Genes Brain Behav. *3*, 287–302.

Nees, F., Witt, S.H., and Flor, H. (2018). Neurogenetic Approaches to Stress and Fear in Humans as Pathophysiological Mechanisms for Posttraumatic Stress Disorder. Biol. Psychiatry *83*, 810–820.

Penzo, M.A., Robert, V., Tucciarone, J., De Bundel, D., Wang, M., Van Aelst, L., Darvas, M., Parada, L.F., Palmiter, R.D., He, M., et al. (2015). The paraventricular thalamus controls a central amygdala fear circuit. Nature *519*, 455–459.

Pfeffer, C.K., Xue, M., He, M., Huang, Z.J., and Scanziani, M. (2013). Inhibition of inhibition in visual cortex: the logic of connections between molecularly distinct interneurons. Nat. Neurosci. *16*, 1068–1076.

Phelps, E.A., and LeDoux, J.E. (2005). Contributions of the amygdala to emotion processing: from animal models to human behavior. Neuron *48*, 175–187.

Pi, H.J., Hangya, B., Kvitsiani, D., Sanders, J.I., Huang, Z.J., and Kepecs, A. (2013). Cortical interneurons that specialize in disinhibitory control. Nature *503*, 521–524.

Rozeske, R.R., Jercog, D., Karalis, N., Chaudun, F., Khoder, S., Girard, D., Winke, N., and Herry, C. (2018). Prefrontal-Periaqueductal Gray-Projecting Neurons Mediate Context Fear Discrimination. Neuron *97*, 898–910.e6.

Rudy, B., Fishell, G., Lee, S., and Hjerling-Leffler, J. (2011). Three groups of interneurons account for nearly 100% of neocortical GABAergic neurons. Dev. Neurobiol. *71*, 45–61.

Sheynin, J., Shind, C., Radell, M., Ebanks-Williams, Y., Gilbertson, M.W., Beck, K.D., and Myers, C.E. (2017). Greater avoidance behavior in individuals with posttraumatic stress disorder symptoms. Stress *20*, 285–293.

Sierra-Mercado, D., Padilla-Coreano, N., and Quirk, G.J. (2011). Dissociable roles of prelimbic and infralimbic cortices, ventral hippocampus, and basolateral amygdala in the expression and extinction of conditioned fear. Neuropsychopharmacology *36*, 529–538.

Somogyi, P., and Klausberger, T. (2005). Defined types of cortical interneurone structure space and spike timing in the hippocampus. J. Physiol. *562*, 9–26.

Soya, S., Takahashi, T.M., McHugh, T.J., Maejima, T., Herlitze, S., Abe, M., Sakimura, K., and Sakurai, T. (2017). Orexin modulates behavioral fear expression through the locus coeruleus. Nat. Commun. *8*, 1606.

Stein, M.B., and Stein, D.J. (2008). Social anxiety disorder. Lancet *371*, 1115–1125.

Taniguchi, H., He, M., Wu, P., Kim, S., Paik, R., Sugino, K., Kvitsiani, D., Fu, Y., Lu, J., Lin, Y., et al. (2011). A resource of Cre driver lines for genetic targeting of GABAergic neurons in cerebral cortex. Neuron *71*, 995–1013.

Toth, I., and Neumann, I.D. (2013). Animal models of social avoidance and social fear. Cell Tissue Res. *354*, 107–118.

Toth, I., Neumann, I.D., and Slattery, D.A. (2012). Social fear conditioning: a novel and specific animal model to study social anxiety disorder. Neuropsychopharmacology *37*, 1433–1443.

Tremblay, R., Lee, S., and Rudy, B. (2016). GABAergic Interneurons in the Neocortex: From Cellular Properties to Circuits. Neuron *91*, 260–292.

Tsien, J.Z., Chen, D.F., Gerber, D., Tom, C., Mercer, E.H., Anderson, D.J., Mayford, M., Kandel, E.R., and Tonegawa, S. (1996). Subregion- and cell type-restricted gene knockout in mouse brain. Cell *87*, 1317–1326.

Xu, H., Jeong, H.Y., Tremblay, R., and Rudy, B. (2013). Neocortical somatostatin-expressing GABAergic interneurons disinhibit the thalamorecipient layer 4. Neuron *77*, 155–167.

Yizhar, O., Fenno, L.E., Prigge, M., Schneider, F., Davidson, T.J., O'Shea, D.J., Sohal, V.S., Goshen, I., Finkelstein, J., Paz, J.T., et al. (2011). Neocortical excitation/inhibition balance in information processing and social dysfunction. Nature *477*, 171–178.

Zelikowsky, M., Hui, M., Karigo, T., Choe, A., Yang, B., Blanco, M.R., Beadle, K., Gradinaru, V., Deverman, B.E., and Anderson, D.J. (2018). The Neuropeptide Tac2 Controls a Distributed Brain State Induced by Chronic Social Isolation Stress. Cell *173*, 1265–1279.e19.

Zhang, W., Zhang, L., Liang, B., Schroeder, D., Zhang, Z.W., Cox, G.A., Li, Y., and Lin, D.T. (2016). Hyperactive somatostatin interneurons contribute to excitotoxicity in neurodegenerative disorders. Nat. Neurosci. *19*, 557–559.

STAR★METHODS

KEY RESOURCES TABLE

REAGENT or RESOURCE	SOURCE	IDENTIFIER
Antibodies		
Rabbit anti-CaMKII	Abcam	Cat# ab52476; RRID: AB_868641
Rabbit anti-parvalbumin	Swant	Cat# PV 27; RRID: AB_2631173
Rabbit anti-somatostatin	Peninsula Laboratories LLC	Cat# T-4103; RRID: AB_518614
Rabbit anti-vasoactive intestinal polypeptide	Immunostar	Cat# 20077; RRID: AB_572270
Rabbit anti-c-Fos	Cell Signaling Technology	Cat# 2250; RRID: AB_2247211
Goat anti-rabbit Alexa Fluor 488	Abcam	Cat# ab150077; RRID: AB_2630356
Goat anti-rabbit Alexa Fluor 594	Abcam	Cat# ab150080; RRID: AB_2650602
Bacterial and Virus Strains		
AAV2/9-hSyn-DIO-GCaMP6m-WPRE-bGHpA	Taitool (Shanghai)	Cat# S0277
AAV2/9-hSyn-DIO-hM3D(Gq)-mCherry	Taitool (Shanghai)	Cat# S0192
AAV2/9-hSyn-DIO-hM4D(Gi)-mCherry	ObioTechnology (Shanghai)	Cat# AG50475
AAV2/9-EF1a-double floxed-EYFP-WPRE-HGHpA	Taitool (Shanghai)	Cat# S0196
AAV2/9-EF1a-double floxed-hChR2 (H134R)-mCherry	BrainVTA (Wuhan)	Cat# PT-0002
Chemicals, Peptides, and Recombinant Proteins		
Fluorescent muscimol	Thermo Fisher Scientific	Cat# M23400
Clozapine-Noxide	Sigma	Cat# C0832
Experimental Models: Organisms/Strains		
Mouse: PV-Cre	Jackson Laboratory; Hippenmeyer et al., 2005	Cat# 008069
Mouse: SST-Cre	Jackson Laboratory; Taniguchi et al., 2011	Cat# 013044
Mouse: VIP-Cre	Taniguchi et al., 2011	Cat# 010908
Mouse: CaMKIIα-Cre	Jackson Laboratory; Tsien et al., 1996	Cat# 005359
Software and Algorithms		
OmniPlex neural recording data acquisition system	Plexon	https://plexon.com/products/omniplex-software
NeuroExplorer	Plexon	https://plexon.com/products/neuroexplorer
Offline sorter	Plexon	https://plexon.com/products/offline-sorter
EthoVision XT video tracking system	Noldus Information Technology	https://www.noldus.com/animal-behavior-research/products/ethovision-xt
MATLAB	MathWorks	https://www.mathworks.com/products/matlab.html
Prism	GraphPad Software	https://www.graphpad.com/scientific-software/prism
ImageJ	National Institutes of Health	https://imagej.nih.gov/ij/index.html

CONTACT FOR REAGENT AND RESOURCE SHARING

Further information and requests for resources and reagents may be directed to and will be fulfilled by the Lead Contact, Han Xu (xuhan2014@zju.edu.cn).

EXPERIMENTAL MODEL AND SUBJECT DETAILS

Male CaMKIIα-Cre, PV-Cre, SST-Cre, VIP-Cre or C57BL/6J wild-type mice (2-4 months old) were used for experiments. Mice were housed under 22 ± 1°C and 55 ± 5% humidity in a 12 h light/dark cycle with food and water *ad libitum*. All animals were group housed

except those experienced social fear conditioning or implanted with chronic microelectrodes. Behavioral experiments were performed during the animals' light cycle. Before behavioral tests, animals were habituated to the experimenter by handling for at least 3 consecutive days (15 min per day). Animal care and use were under the guidelines approved by the Animal Care and Use Committee of Zhejiang University.

METHOD DETAILS

Social Fear Conditioning Paradigm

The social fear conditioning (SFC) was performed with a computerized fear conditioning system (Figure 1A). The conditioning chamber consisted of a white Plexiglas box (30 cm long, 30 cm wide and 50 cm high) enclosed in a metallic chamber to reduce external sensory disturbance. The floor consisted of an unmovable stainless steel grid connected to a shock delivery unit for foot shocks. The experimental mouse was first placed in the conditioning chamber with two identical empty cages at two opposing corners. After a 5 min of acclimation period, an unfamiliar male stimulus mouse was placed in one of the cages, and experimental mouse was allowed to explore the stimulus mouse for 2 min. Then during a 20 min social fear conditioning period, the experimental mouse was given an electric foot shock (1 s, 0.6 mA) each time as it investigated the stimulus mouse, defined by direct contact with the stimulus mouse (Figure 1A; Video S1).

Our conditioning paradigm was in principle adapted from the one proposed by Toth et al. (2012), but with several significant modifications. First, instead of visual inspection of social contacts and manual application of foot shocks by Toth et al. (2012), individual social contacts were detected and electric shocks were delivered automatically with a computerized fear conditioning unit equipped with video tracking system. This modification is to ensure consistency of conditioning criteria and therefore supposedly to reduce the behavioral variation among conditioned subjects. Second, we placed two identical cages on each of two opposing corners of the conditioning chamber. One cage was empty and the other contained a stimulus mouse. Such arrangement is to facilitate fear acquisition specifically to stimulus mouse but not to the cage. Indeed, conditioned mice did not show any signs of fear to the cage itself during conditioning or afterward. Third, we extended conditioning procedure to a longer duration (20 min) even though the experimental mouse typically did not approach stimulus mouse and get foot shocks any more after 5 min. This modification is inspired by the observation that staying physically close to a social stressor helps to reinforce behavioral adaption in social defeat paradigm (Golden et al., 2011).

Three-Chamber Social Interaction Test

Animals were allowed to acclimate to the behavioral testing room for at least 1 h before the first trial began. The apparatus consisted of a three-compartment (Length: 20 cm; Width: 40 cm; Height: 20 cm for each) white Plexiglas box. Dividing walls were made from clear Plexiglas, with rectangular openings (10 cm in width and equipped with sliding doors) in the middle to enable free access to each chamber. Two identical inverted wire cups (diameter 10 cm, Galaxy Pencil Cup) were placed in the corner of each side compartment (one per each site) during testing sessions. A test mouse was then placed in the middle compartment and was allowed to freely explore the apparatus for 10 min. After this habituation period, an unfamiliar stimulus mouse of the same age, sex and strain was placed inside the wire cup in one of the side compartments designated as the social chamber and the opposite compartment with an empty wire cup was designates as the neutral chamber. Social chamber was randomly selected and counterbalanced for each group. The test mouse was allowed to freely explore all three compartments of the apparatus for another 10 min. Mouse overall activity in the apparatus was automatically recorded by a video camera, and the EthoVision XT video tracking system (Noldus, Netherland) was used to track mouse location and movement of head and body. The amount of time that test mouse spent in each chamber was measured. The social interaction index calculated as the difference in the time spent in the social and neutral chambers, divided by the sum of the time spent in both chambers. Social approach times, approach speed and stretched postures behavior were quantified during the 10 min interaction period. After each session, the apparatus and wire cups were thoroughly cleaned with 75% ethanol to prevent olfactory cue bias.

Social Preference-Avoidance Test

Animals were allowed to acclimate to the behavioral testing room for at least 1 h before the first trial began. A test mouse was then placed in an open field arena (40 cm long, 40 cm wide and 40 cm high) with an empty wire cage and was allowed to freely explore the apparatus for 10 min. After this habituation period, unfamiliar male or female stimulus mouse of the same age and strain or an object (plastic Lego) was placed inside the wire cup. The test mouse was allowed to freely explore the arena for another 10 min. Mouse overall activity in the apparatus was automatically recorded by a video camera, and the EthoVision XT video tracking system was used to track mouse location and movement of head and body. Total distance and amount of time spent in the immediate vicinity (8 cm) of the cage were measured. Social approach times, approach speed and stretched postures behavior were quantified during the 10 min interaction period. After each session, the apparatus and wire cups were thoroughly cleaned with 75% ethanol to prevent olfactory cue bias.

Open Field Test

The open field test was used to measure anxiety-like behavior and locomotor activity in an open field arena (40 cm long, 40 cm wide and 40 cm high). The total distance traveled, time spent in center zone and number of center entries were recorded and analyzed for 10 min using EthoVision XT. The arena was cleaned with 75% ethanol between tests.

Forced Swim Test

Animals were individually placed in a cylinder (11 cm diameter, 30 cm height) of water (23–25°C) and swam for 6 min under normal light. Water depth was set to prevent animals from touching the bottom with their tails or hind limbs. Animal behaviors were videotaped from the side. The immobile time during the last 4-min test was counted offline by an observer blinded to animal treatment. Immobile time was defined as time when animals remained floating or motionless with only movements necessary for keeping balance in the water.

Social Defeat Paradigm and Social Fear Test

For three consecutive days, an aggressive male CD1 intruder mouse was introduced to the home cage of singly-housed adult C57 male mice for 15 min per day. The intruder was confined within a wire cup for 5 min and then was allowed to attack the resident repeatedly. Control animals were treated in the same way except that the wire cup was not removed. This allowed control mice similar levels of sensory contact with the aggressor as defeated mice. A week after the last social defeat session, mice were subjected to a social preference-avoidance test in which an unfamiliar aggressive CD1 intruder was confined within a wire cup at one end of the open field. Time spent in social zone and corner within 5 min were recorded and analyzed using EthoVision XT.

Drug Infusion

Fluorescent muscimol (MUS, BODIPY TMR-X conjugate) was used to activate GABAa receptors and hence to inactivate target structures, and was administered 30 min prior to social fear expression. MUS or PBS was infused at a rate of 200 nl/min for PrL (0.25 nmol/150 nl/side) or BLA (0.11 nmol/200nl/side) according to previous studies (Do-Monte et al., 2015; Sierra-Mercado et al., 2011).

Virus Injection

GCaMP6m (AAV2/9, 3.36×10^{12} genomic copies per ml), hM3D (AAV2/9, 3.43×10^{12} genomic copies per ml), hM4D (AAV2/9, 3.44×10^{12} genomic copies per ml), hChR2(AAV2/9, 3.26×10^{12} genomic copies per ml), EYFP (AAV2/9, 5.54×10^{12} genomic copies per ml) were made by Taitool (Shanghai), Obio Technology (Shanghai) or BrainVTA (Wuhan). CaMKIIα-Cre, PV-Cre, SST-Cre or VIP-Cre mice (8-9 weeks old) were anesthetized with isoflurane (induction 4%, maintenance 1%) and placed in a stereotaxic frame (Stoelting Co., IL, USA). The skull was exposed under antiseptic conditions and a small craniotomy was made with a thin drill over prefrontal cortex (typical coordinate: 1.9 mm posterior to Bregma; 0.3 mm lateral to the midline). AAVs carrying fusion genes for GCaMP6m (AAV-hSyn-DIO-GCaMP6m-WPRE-bGHpA), hM3D (AAV-hSyn-DIO-hM3D(Gq)-mCherry), hM4D (AAV-hSyn-DIO-hM4D(Gi)-mCherry), hChR2(AAV-EF1a-double floxed-hChR2 (H134R)-mCherry) or EYFP (AAV-EF1a-DIO-EYFP) were injected using a glass micropipette (tip diameter ~15 μm) attached to a Nanoliter 2000 pressure injection apparatus (World Precision Instruments). Over a 5 min period, 100-200 nL of virus was injected at a depth of 2.1 mm from the Bregma. The pipette remained for 10 min at the end of infusion to allow virus diffusion. Viruses were injected bilaterally for behavioral manipulation and unilaterally for fiber photometry or optogenetic tagging of inhibitory neurons. Experiments were conducted at least 4 weeks after virus injection.

Surgical Implantation of Tetrodes

After a craniotomy (0.8-1.0 mm in diameter) was made and the dura mater was removed, a custom-made 8 movable tetrodes array was inserted into the dmPFC (coordinates: 1.9 mm anterior, 0.4 mm lateral and 1.8-2.5 mm ventral from Bregma). Each tetrode was made of four twisted fine platinum/iridium wires (12.5 μm diameter, California Fine Wire) and threaded through a silica tube (75 μm inner, 152 μm outer diameter; Polymicro Technologies). The micro-wire tips underwent final cutting with a serrated fine scissor, and then were plated with gold by passing cathodal current to reduce impedance to a final value of 300-400 kΩ at 1 kHz. Each wire was soldered to a 36-pin connector (Omnetics Connector), and the other four pins were soldered with two pairs of copper micro-wires (~100 μm diameter) for grounding and reference. The whole implant was fixed to the skull with four miniature skull screws, cyanoacrylate glue and dental cement. Mice were then placed on a heating pad to wake up and thereafter single-housed.

Optogenetic Tagging of PV INs

For *in vivo* optogenetic tagging of PV INs, PV-Cre mice were unilaterally injected with AAV DIO ChR2-mCherry aimed at mPFC (Cardin et al., 2009). Four weeks later, optrodes were implanted at the same coordinates by which virus was injected. The optrodes consisted of one optic fiber surrounded by multiple tetrodes, with the tip protruding ~300 μm beyond the fiber (Figure S6). The tetrodes were lowered gradually by ~40 μm after each daily test to record different units. For optical identification of PV INs, blue light pulses (470 nm, 1-2 ms duration, 0.08-1.35 mW at fiber tip) were delivered at the end of each recording session at high frequencies (20 Hz). Units were considered as light responsive if they exhibited time-locked spiking with high reliability (> 90%), short first-spike latency (< 3 ms) and low jitter (< 2 ms) upon light pulses illumination. Only when the waveforms of laser-evoked and spontaneous spikes were highly similar (correlation coefficient > 0.9), they were considered to originate from the same neuron.

Electrophysiological Data Acquisition during Social Fear Expression

After a 7-day recovery from the surgery, mice were habituated to the headstage and cables connected to the electrode on their heads for several days prior to electrophysiological recordings. To ensure that animals could move freely, the connecting cable was suspended over the behavioral apparatus using a nitrogen balloon. To explore dmPFC neuronal activity during social fear expression, recordings were performed when subject mouse was freely exploring a one-chamber social interaction apparatus (Length: 20 cm; Width: 40 cm; Height: 20 cm) (Figure 3). A small cylinder-shaped acrylic cage was placed at the middle of one side; a subject mouse was placed at the opposite side of the apparatus and allowed to acclimate for 10 min. Then an unfamiliar same-gender stimulus mouse was confined within the cylinder cage. Subject animals were allowed to freely explore the entire apparatus for another 10 min without any disturbance, and multichannel electrical signals were recorded throughout this period. Spiking activities were digitized at 40 kHz, bandpass filtered from 250 Hz to 8000 Hz, and stored on a PC for further offline analysis. Animals' behavior was monitored throughout the testing session with a digital camera right above (100 cm higher) the center of the apparatus, and video was simultaneously recorded and aligned with the electrophysiological recordings for offline analysis (Plexon Inc.).

Spike Sorting

The single unit spike sorting was performed with Offline Spike Sorter software (Plexon Inc.). Spikes were identified when a minimum waveform reached an amplitude threshold of 3 standard deviations higher than the noise amplitude. Principal component analysis (PCA) was employed to automatically separate waveforms into individual clusters. Manual checking was then performed to ensure that the spike waveforms were consistent and that the cluster boundaries were clearly separated. All isolated single units exhibited recognizable refractory periods (> 2 ms) in the inter-spike interval (ISI) histograms. Only well-isolated units (L ratio < 0.2, isolation distance > 15) were included in the data analysis.

Unit Classification and Firing Rate Analysis

The well-isolated units were first classified into wide-spiking (WS) putative pyramidal neurons and narrow-spiking (NS) INs using unsupervised cluster algorithm based on κ-means method. The analysis was based on the three-dimensional space defined by each neuron's half-spike width (trough to peak duration), half valley width and the mean firing rate at baseline (Figure S6). Spikes with shorter half-spike width, half valley width and higher firing rate were classified to be putative INs. The NS population was further classified into putative FS-PV INs (> 10 Hz) and non-FS NS neurons based on baseline firing rate (Courtin et al., 2014; Kim et al., 2016a). Spike rate during a 2 s period right before the onset of a risk assessment was defined as baseline firing rate, and that during a 2 s period right before the retreat from the stimulus mouse was defined as fear expression firing rate. Then the spike rates from multiple risk assessments (> 5) were averaged to calculate a mean firing rate for both baseline and fear expression. For a given neuron, firing rates during fear expression and during baseline were compared to determine the significance of firing rate difference between these two conditions (paired t test). To ensure accuracy, only risk assessments with duration of longer than 2 s and an interval from previous visit of more than 2 s were used for spike rate analysis.

Neuronal Responses to Pharmacogenetic Manipulations

To determine the effect of pharmacogenetic activation/inactivation on neuronal activity of different types of neurons, CaMKIIα-Cre or SST-Cre mice were unilaterally injected with AAV-DIO-hM4D-mCherry, and PV-Cre mice were injected with AAV-DIO-hM3D-mCherry virus aimed at dmPFC. Four weeks later, tetrodes were implanted at the same coordinate as the one for virus injection. Mice were habituated with recording headstage and cable for at least 30 min and the baseline firing rates were recorded in their homecages. Then CNO (1 or 5 mg/kg) was injected intraperitoneally, and electrophysiological data was recorded 1.5 hr after CNO administration. As for CaMKIIα-Cre::hM4D and PV-Cre::hM3D mice, putative pyramidal cells and FS-PV INs were identified based on spike waveforms and spike rates. As for SST-Cre::hM4D mice, neurons with a significant decrease in firing rate following CNO administration were considered as putative SST INs. Only if the spikes were highly similar in waveforms (correlation coefficient > 0.9) before and after CNO administration, they were considered to originate from the same neuron.

Fiber Photometry

Following AAV-DIO-GCaMP6m virus injection, an optical fiber (230 μm O.D., 0.37 numerical aperture (NA); Newdoon Inc.) was placed in a ceramic ferrule and inserted toward the PrL through the craniotomy. The ceramic ferrule was supported with a skull-penetrating M1 screw and dental acrylic. Mice were individually housed for at least 1 week to recover. Fiber photometry system (ThinkerTech, Nanjing) was used to record calcium signals from genetically identified INs including SST and VIP INs. Specifically, to record fluorescence signals, laser beam from a 488-nm laser (OBIS 488LS; Coherent) was reflected by a dichroic mirror (MD498; Thorlabs), focused by a x10 objective lens (NA = 0.3; Olympus) and then coupled to an optical commutator (Doric Lenses). An optical fiber (230 μm O.D., NA = 0.37, 2 m long) guided the light between the commutator and the implanted optical fiber. The laser power was adjusted at the tip of optical fiber to a low level of 0.01-0.02 mW, to minimize bleaching. The GCaMP fluorescence was bandpass filtered (MF525-39, Thorlabs) and collected by a photomultiplier tube (R3896, Hamamatsu). An amplifier (C7319, Hamamatsu) was used to convert the photomultiplier tube current output to voltage signals, which was further filtered through a low-pass filter (40 Hz cut-off; Brownlee 440). The analog voltage signals were digitalized at 500 Hz and recorded by a Power 1401 digitizer and Spike2 software (CED, Cambridge, UK).

Pharmacogenetic Inactivation during Behavior

Clozapine-N-Oxide (CNO, C0832, Sigma) was dissolved in saline (0.9% NaCl solution) to a working concentration of 0.15 mg/ml or 0.75 mg/ml and stored at −20°C. For pharmacogenetic inactivation of CaMKII neurons, CNO (1 mg/kg body weight) was administered intraperitoneally (i.p. injection) to the hM4D transfected mice 1.5 h prior to behavioral testing. For pharmacogenetic activation of PV INs, CNO (5 mg/kg body weight) was administered intraperitoneally (i.p. injection) to the hM3D transfected mice 1.5 h prior to behavioral testing. For pharmacogenetic inactivation of SST INs, CNO (5 mg/kg body weight) was administered intraperitoneally (i.p. injection) to the hM4D transfected mice 1.5 h prior to behavioral testing. To avoid potential confounding effect of CNO metabolite, the same amount of CNO was administered to EYFP transfected control animals as comparison.

Immunohistochemistry

Mice were transcardially perfused with 20 mL phosphate-buffered saline (PBS), followed by 30 mL 4% paraformaldehyde in 0.1 M PB (pH 7.4). Dissected brains were post-fixed in 4% paraformaldehyde in 0.1 M PB for 2 h at 4°C and then placed in a 30% sucrose solution at 4°C until the brains sank. Using a cryostat (Leica CM1950), 40-μm-thick coronal sections were collected in PBS. Sections were washed in PBS two times (15 min each time) and then incubated with blocking solution (10% normal goat serum, 1% BSA, 0.2% cold fish gelatin, and 0.3% Triton X-100 in PBS) for 1 h at room temperature. Sections were then incubated with primary antibody in diluted (1:10) blocking solution overnight at 4°C. The following primary antibodies were used: rabbit anti-CaMKII (1:300; Abcam, ab52476), rabbit anti-parvalbumin (1:1000; Swant, PV 27), rabbit anti-somatostatin (1:1000; Peninsula Laboratories LLC, T-4103), rabbit anti-vasoactive intestinal polypeptide (1:250; Immunostar, 20077), rabbit anti-c-Fos (1:1000; CST, 2250). After washing in diluted (1:10) blocking solution three times (15 min each time), sections were then incubated with species-specific fluorophore-conjugated secondary antibodies (1:1000; goat anti-rabbit Alexa Fluor 488 or 594, Abcam, ab150077 or ab150080) in diluted (1:10) blocking solution for 2 h at room temperature. After washing in PBS three times (15 min each time), sections were mounted on glass slides with Vectashield (Vector Laboratories) and coverslipped. Using a confocal microscope (Olympus FV1200) with a 10X or 20X objective, images were acquired to verify virus expression and for cell counting. Scans from each channel were collected in multi-track mode to avoid cross-talk between channels. For c-Fos immunostaining, mice were perfused 90 min after social fear expression, 3 sections were collected per mouse and images were acquired using a fluorescent microscope (Olympus, VS120) at a 10X objective. Cell counts were was performed with ImageJ software.

QUANTIFICATION AND STATISTICAL ANALYSIS

All data are shown as mean ± SEM unless otherwise specified. Statistical analyses were done with Prism 7 (GraphPad) or MATLAB. Animal behaviors were video recorded and analyzed with EthoVision XT (Noldus). Comparisons were conducted with Student's t test or two-way ANOVA followed by Bonferroni's post-tests for multiple comparisons where appropriate. $p < 0.05$ was considered statistically significant. *$p < 0.05$, **$p < 0.01$, ***$p < 0.001$, ****$p < 0.0001$.